# A Comprehensive Evaluation and Analysis of the Performance of Multiple Tropospheric Models in China Region

Biyan Chen, *Student Member, IEEE*, and Zhizhao Liu

***Abstract*—Tropospheric path delay is an important error source in range measurements of many Earth observation systems. In this paper, the accuracies of 9 zenith hydrostatic delay (ZHD) and 18 zenith wet delay (ZWD) models are assessed using benchmark values derived from 10 years (2003–2012) of radiosonde data recorded at 92 stations in the China region. Our study confirms that ZHD can be well modeled with an accuracy of several millimeters by using surface meteorological observations. ZHD derived from the European Center for Medium-Range Weather Forecasts (ECMWF) has the best agreement of 2.8 mm with the radiosonde data in the China region, while the Baby ZHD model achieves the second best with an accuracy of 6.0 mm. All of the ZWD models can only estimate the ZWD with an accuracy of a few centimeters. ECMWF can provide ZWD estimation with the best accuracy of 21.4 mm, followed by the Baby semiempirical, Hopfield, Goad and Goodman, Askne and Nordius, Saastamoinen, Callahan, and Berman 74 ZWD models whose errors are below 40 mm. We find that in the China region all of the ZWD models perform better in winter than in summer and have higher accuracy in high latitudes than low latitudes. The performances of the 18 ZWD models are further validated in a Global Positioning System (GPS) precise point positioning (PPP) computation at 6 GPS stations in China. The PPP results also confirm that ECMWF is the best model. Considering its performance and simplicity, we conclude that Saastamoinen is the optimal ZWD model for the China region.**

***Index Terms*—Performance evaluation, radiosonde, tropospheric delay, zenith hydrostatic delay (ZHD) model, zenith wet delay (ZWD) model.**

## I. Introduction

THE presence of terrestrial atmosphere can cause path delays to radio signals as they transmit from satellites or quasars to the surface of the Earth. Tropospheric delay is a major error source in many space geodetic techniques such as the very long base interferometry, satellite altimetry, satellite laser ranging, interferometric synthetic aperture radar (InSAR), and Global Navigation Satellite System (GNSS) [1]–[8]. Tropospheric path delay, commonly reaching a value of 2.3 m in the zenith, can be divided into two parts: a hydrostatic component and a wet component [9]. The hydrostatic delay is induced by dry gases of the air and accounts for more than 90% of the total tropospheric delay [9]. The wet delay is due to water vapor in the atmosphere and usually contributes less than 10% of the total tropospheric delay [9].

To achieve a high level of observation accuracy using these geodetic techniques, the tropospheric delay must be compensated properly. Over the past few decades, many empirical tropospheric models have been developed to estimate tropospheric hydrostatic and wet delays [9]–[11]. These models provide a convenient and effective way to correct tropospheric delays and have been widely used in many geodetic techniques such as GNSS positioning and InSAR [1], [11]. Compared to the hydrostatic delay, it is more difficult to model the wet delay because of the high variability of water vapor in both spatial and temporal domains [1], [9], [12], [13].

The availability of a large number of tropospheric models offers users great flexibility of choice in their applications. However, a practical problem is that which model is the most accurate or suitable one under a particular observation environment. For different applications, the observation environments, including the user geographical location, altitude of observation site, type of applications (real time or postmission), observation season/time, and availability of auxiliary data such as temperature, pressure, and relative humidity, may vary significantly. The atmospheric properties, particularly the water vapor that is a primary contributor to wet delay, vary considerably from location to location [14]. For different applications, the requirements for tropospheric models are different too. In satellite altimetry, altimetry measurements are required to have an accuracy of a few (1–3) centimeters in order to monitor the ocean dynamics [15], [16]. In GNSS meteorology, the accuracy of the hydrostatic model is the most important consideration since the precipitable water vapor directly depends on the performance of the hydrostatic model. In some GNSS applications where meter-level accuracy is acceptable, the users may be more concerned with the time than the accuracy. Thus, the convenience of using a tropospheric model is more important than its accuracy.

The straightforward way to correct the tropospheric effect in range observations is to use a tropospheric model in combination with necessary meteorological data that are obtained from ground observations or from other models [17]. Accuracy of centimeter level is achievable if the proper tropospheric model

Manuscript received November 14, 2014; revised February 9, 2015, April 14, 2015, and May 15, 2015; accepted June 16, 2015. Date of publication September 28, 2015; date of current version January 19, 2016. This work was supported by the National Natural Science Foundation of China (41274039) and the Hong Kong Research Grants Council (RGC) General Research Fund (GRF) project PolyU 5217/11E (B-Q28F). *(Corresponding author: Zhizhao Liu.)*

The authors are with the Department of Land Surveying and Geo-Informatics, The Hong Kong Polytechnic University, Kowloon, Hong Kong (e-mail: 12901813r@connect.polyu.hk; lszzliu@polyu.edu.hk).

Color versions of one or more of the figures in this paper are available online at http://ieeexplore.ieee.org.

Digital Object Identifier 10.1109/TGRS.2015.2456099

is selected [18]. However, an improperly selected tropospheric model may severely degrade the performance of tropospheric delay compensation. It is thus necessary to comprehensively and systematically investigate the performance of each tropospheric model under various conditions before it is employed in practice.

A lot of studies have been conducted to evaluate the performances of different tropospheric models. Janes *et al.* evaluated two hydrostatic delay models and six wet delay models based on benchmark values derived from the U.S. Standard Atmosphere and the U.S. Standard Atmosphere Supplements [19]. By using one-year's radiosonde data from 50 globally distributed stations, Mendes systematically assessed the performances of 4 hydrostatic delay models and 12 wet delay models [9]. In that research, it was found that the Saastamoinen model has the best global accuracy in the estimation of both hydrostatic and wet troposphere delays. Li *et al.* conducted a systematic research on the zenith tropospheric delay with three-year radiosonde data recorded at one station in Hong Kong [11]. Research results showed that the Askne and Nordius model performed best and the Saastamoinen model achieved a relatively poor accuracy in the Hong Kong region. Qu *et al.* compared the tropospheric delay corrections derived from the Saastamoinen, Hopfield, and EGNOS models with zenith tropospheric delay data obtained from 36 globally distributed International GNSS Service (IGS) stations, and they indicated that the EGNOS model can be applied in GNSS real-time positioning and navigation [20]. Dodo and Idowu assessed the performances of three tropospheric delay models for the African GNSS network, and they found that the refined Saastamoinen model performed better than the modified Hopfield and Niell model [21]. Recently, Tuka and El-Mowafy have conducted a study to compare the performances of several hydrostatic delay and wet delay models at six selected IGS stations [22]. In their comparison, they used the Saastamoinen model as reference and indicated that all of the models employed in their study could achieve better performance at midlatitude regions than at the equator.

China has a massive GNSS market and is progressively developing the Chinese BeiDou Navigation Satellite System (BDS) [23]. With the rapid progress of the BDS, the number of Global Positioning System (GPS) and BDS users is growing significantly. One typical example is the extraordinarily large number of GNSS-enabled smartphone users in China. It is expected that the GNSS users (including BDS users) will continue to grow in the next years. However, over the years, no study has been conducted to comprehensively evaluate the performances of different tropospheric models for the China region. Some of the works discussed previously focused on local applications (e.g., [11] and [21]) but not the China region. Global performance evaluation of different tropospheric models has been conducted (e.g., [9] and [22]). However, the China region was not a focus in those studies. The massive GNSS user market and the large landmass covering various climate zones in China demand an investigation of which tropospheric model can provide the most accurate corrections. Furthermore, more and more GNSS meteorology applications are being developed in China [24]–[26], in which precise tropospheric hydrostatic modeling is needed in order to retrieve water vapor data precisely. Identifying the most precise hydrostatic model is thus also very valuable for the China region.

TABLE I
REFRACTIVITY CONSTANTS (FROM [31])

| $k_1$ (K/hPa) | $k_2$ (K/hPa) | $k_3$ (K$^2$/hPa) |
|---|---|---|
| 77.6890 | 71.2952 | 375463 |

This study presents a comprehensive evaluation of the performances of 9 hydrostatic and 18 wet delay models with respect to reference hydrostatic and wet delays, respectively. The reference delays are derived from radiosonde data collected at 92 stations in China over a 10-year period from 2003–2012. In addition to the overall performance, we also assess their temporal performance in different seasons and spatial performance at various latitude zones. In order to validate the performances of the tropospheric models through a real-world application, a further study is carried out to apply these models in a kinematic GPS precise point positioning (PPP) application. This is achieved by utilizing the tropospheric models to correct tropospheric delay of GPS data in the PPP computation. The work presented in this paper will provide valuable references for many users and applications of the tropospheric models, particularly for the massive GNSS users and manufacturers in China.

This paper is structured as follows. In Section II, we will introduce the method to derive hydrostatic and wet delays from radiosonde data. Section III describes nine hydrostatic and 18 wet delay models to be studied in this work. An introduction of the radiosonde measurement and its accuracy analysis is presented in Section IV. The performances of the tropospheric models with respect to radiosonde data and in kinematic PPP are discussed in Section V. The conclusion and final remarks are given in Section VI.

## II. THEORETICAL BACKGROUND FOR TROPOSPHERIC DELAY

In the zenith direction, the total tropospheric delay can be expressed as [27]

$$\Delta L = 10^{-6} \int_{H}^{\infty} N \cdot d_z \tag{1}$$

where $\Delta L$ is the total tropospheric delay (unit: meters), $H$ is the height of the observation station over mean sea level (unit: meters), $N$ is the atmospheric refractivity (unitless) that can be modeled as follows [28]:

$$N = k_1 \cdot \frac{P_d}{T} + k_2 \cdot \frac{e}{T} + k_3 \cdot \frac{e}{T^2} \tag{2}$$

where $P_d$ and $e$ are the dry air and water vapor partial pressures (unit: hectopascals), respectively, $T$ is the temperature (unit: kelvin), and $k_1$, $k_2$, and $k_3$ are the refractivity constants, and their values used in this study are listed in Table I. The water vapor partial pressure $e$ can be derived as follows [29], [30]:

$$e = 6.1121(1.0007 + 3.46 \times 10^{-6} \cdot P) \cdot RH \cdot \exp\left\{\frac{[18.729 - (T - 273.15)/227.3](T - 273.15)}{T - 15.28}\right\} \tag{3}$$

where $P$ is the total pressure (unit: hectopascals) and $RH$ is the relative humidity (unitless).

Using the equation of state, we can express the air density $\rho$ as [9]

$$\rho = \frac{P_d}{T \cdot R_d} + \frac{e}{T \cdot R_w} \tag{4}$$

where $P_d$, $T$, and $e$ have been defined in (2); $R_d = 287.053\ \mathrm{J} \cdot \mathrm{K}^{-1} \cdot \mathrm{kg}^{-1}$ and $R_w = 461.495\ \mathrm{J} \cdot \mathrm{K}^{-1} \cdot \mathrm{kg}^{-1}$ are the gas constants for dry air and water vapor, respectively. The hydrostatic refractivity $N_h$ can be calculated as

$$N_h = k_1 R_d \rho. \tag{5}$$

Considering (2), (4), and (5), we derived the wet refractivity $N_w$

$$N_w = \left(k_2 - k_1 \frac{R_d}{R_w}\right) \cdot \frac{e}{T} + k_3 \frac{e}{T^2}. \tag{6}$$

Substituting (5) and (6) into (1), we get

$$\Delta L = 10^{-6} \int_H^\infty N_h \cdot d_z + 10^{-6} \int_H^\infty N_w \cdot d_z. \tag{7}$$

The first term at the right-hand side of (7) is termed tropospheric hydrostatic delay. The last term in (7) is known as tropospheric nonhydrostatic delay. For the sake of convenience, we use the term "wet delay" to substitute the "nonhydrostatic delay," although this term is not very precise as the hydrostatic delay also contains a small contribution from the wet delay. In this paper, the reference values for both hydrostatic and wet delays are obtained from radiosonde data. They are used as benchmark to evaluate the performances of various tropospheric hydrostatic and wet models. The radiosonde sensors can measure several meteorological parameters such as the pressure, temperature, and relative humidity. Taking the characteristic of exponential decreasing of the atmospheric refractivity into account, the formulas for zenith hydrostatic and wet delays from the radiosonde measurements can be derived

$$\Delta L_h = 10^{-6} \sum_i \left[ \frac{(H_i - H_{i+1})\left(N_{h_{i+1}} - N_{h_i}\right)}{\left(\ln N_{h_i} - \ln N_{h_{i+1}}\right)} \right] \tag{8}$$

$$\Delta L_w = 10^{-6} \sum_i \left[ \frac{(H_i - H_{i+1})\left(N_{w_{i+1}} - N_{w_i}\right)}{\left(\ln N_{w_i} - \ln N_{w_{i+1}}\right)} \right] \tag{9}$$

where $\Delta L_h$ and $\Delta L_w$ are the zenith hydrostatic delay (ZHD) and zenith wet delay (ZWD) (unit: meters), respectively, and $H_i$ denotes the height of a given layer $i$ (unit: meters). $N_{h_i}$ and $N_{w_i}$ are the hydrostatic and wet refractivity values at a given layer $i$, respectively.

## III. Descriptions of Tropospheric Hydrostatic and Wet Models

Several studies have shown that the calculation formula for the hydrostatic delay is theoretically derivable based on the assumption that the air is an ideal gas and that the troposphere satisfies the hydrostatic equilibrium [27], [32], [33]. The ZHD can be calculated by

$$\Delta L_h = 10^{-6} k_1 R_d \frac{P_s}{g_m} \tag{10}$$

where $k_1$ and $R_d$ have been defined in (2) and (4), respectively, $P_s$ is the atmospheric pressure at the surface (unit: hectopascals), and $g_m$ is the gravity acceleration at the centroid of the vertical atmosphere column (unit: meters per square second). Substituting the gas constant $R_d = 287.053\ \mathrm{J} \cdot \mathrm{K}^{-1} \cdot \mathrm{kg}^{-1}$ and the constant $k_1$ given in Table I into (10), we can rewrite the ZHD as

$$\Delta L_h = 0.0223009 \cdot \frac{P_s}{g_m}. \tag{11}$$

It can be noted that the hydrostatic delay is a function of surface pressure $P_s$ and the gravity acceleration $g_m$. The surface pressure can be measured by using a barometer with a high accuracy. Thus, most of the ZHD models mainly focus on the accurate modeling of gravity acceleration $g_m$.

Meanwhile, a large number of tropospheric wet delay models have also been developed in the past decades. ZHD can be modeled with a reasonably good accuracy using surface meteorological data (to be shown in Section V); nevertheless, the ZWD is often difficult to be modeled accurately even using surface meteorological parameters [9]. This is attributed to the nature of atmospheric water vapor that is highly variable in both space and time domains. Because of this, a comprehensive evaluation of the performances of the ZWD models becomes even more crucial than the ZHD models. In the following sections, the 9 ZHD and 18 ZWD models to be evaluated in this study are described. From Sections III-A–H, the models can be used to calculate ZHD and ZWD. However, the models described in Sections III-I–M can only be used to compute ZWD. Please note that, in some sections, more than one model is described.

### A. Saastamoinen Model

For the ZHD calculation formula in (11), Saastamoinen found that the $g_m$ can be approximately determined using the expressions as follows [32]:

$$g_m = 9.784 \cdot f(\varphi, H) \tag{12}$$

$$f(\varphi, H) = 1 - 0.0026 \cdot \cos(2\varphi) - 2.8 \times 10^{-7} \cdot H \tag{13}$$

where $\varphi$ is the station latitude (unit: radians) and $H$ is the height of the station above sea level (unit: meters). Equation (11) can be rewritten by considering (12) and (13)

$$\Delta L_h = 0.0022793 \cdot \frac{P_s}{f(\varphi, H)}. \tag{14}$$

In the derivation of the ZWD model, Saastamoinen assumed that the variation of water vapor pressure $e$ can be described by the following expression [34]:

$$e = e_s \cdot \left(\frac{T}{T_s}\right)^{\frac{v \cdot g}{R_d \cdot \alpha}} \tag{15}$$

where $e_s$ is the water vapor pressure at the surface level (unit: hectopascals), $T$ is the temperature (unit: kelvin), $T_s$ is the surface temperature (unit: kelvin), $v$ is a numerical coefficient to be determined from local observations (unitless), $g$ is gravity acceleration (unit: meters per square second), $R_d$ is the same defined in (4), and $\alpha$ refers to the temperature lapse rate (unit: kelvin per kilometer) with a standard temperature lapse rate of 6.5 K/km. Combining (15) and (6) and integrating with respect to height, the Saastamoinen ZWD model is obtained

$$\Delta L_w = 0.002277 \cdot \left(\frac{1255}{T_s} + 0.05\right) \cdot e_s. \tag{16}$$

### B. Baby Model

Considering that gravity acceleration decreases with altitude, Baby *et al.* derived the $g_m$ as follows [35]:

$$g_m = \frac{g_s}{1 + 2T_s/\left[r_s\alpha(\mu+1)\right]} \tag{17}$$

where $g_s$ is the surface gravity acceleration at the station (unit: meters per square second), $T_s$ is the surface temperature (unit: kelvin), $r_s$ is the distance from the center of the Earth to the station (unit: meters), and $\alpha$ has been defined in (15). $\mu$ is calculated using the following expression [35]:

$$\mu = \frac{g_s r_s}{R_d(r_s\alpha - 2T_s)}. \tag{18}$$

Integrating (11), (17), and (18), we can obtain

$$\Delta L_h = 0.0223009\frac{P_s}{g_s} \cdot \left[1 + \frac{2T_s \cdot R_d(r_s\alpha - 2T_s)}{r_s\alpha\left[g_s r_s + R_d(r_s\alpha - 2T_s)\right]}\right]. \tag{19}$$

For the ZWD model, Baby *et al.* assumed that the relative humidity $RH$ is constant up to a height $H_m$, where it decreases to zero [35]. Based on this assumption, the saturation water vapor pressure $P_{wvs}$ is expressed in the following form [35]:

$$P_{wvs} = \exp\left(A - \frac{B(T)}{T}\right) \tag{20}$$

where $A$ and $B$ are coefficients. They obtained that $A = 21.3195$ and $B(T) = 5\,327.1157$ when $T > 273.15\,^{\circ}$K, and $A = 24.3702$ and $B(T) = 6\,162.3496$ when $T \leq 273.15\,^{\circ}$K. Assuming that the temperature $T$ decreases with height at a constant rate $\alpha$, Baby *et al.* obtained the following closed-form formula for the $\Delta L_w$ [35]:

$$\Delta L_w = 3.81 \cdot \frac{RH}{\alpha} \cdot \left[\frac{P_{wvs}(T_s)}{B(T_s)} - \frac{P_{wvs}(T_m)}{B(T_m)}\right] \tag{21}$$

where $B(T_s)$ is the value of $B$ corresponding to the temperature measured at the ground surface, denoted as $T_s$, and $B(T_m)$ is the value of $B$ corresponding to the temperature at height $H_m$, denoted as $T_m$.

Baby *et al.* also proposed a semiempirical model for the wet delay to replace the theoretical model given previously. This semiempirical model is suitable for regions where water vapor experiences larger variations [35]. The general expression for the semiempirical model of the wet delay is

$$\Delta L_w = v \cdot 10^{\gamma\cdot(T_s - 273.15)} \cdot RH \tag{22}$$

where $v$ and $\gamma$ are empirical coefficients that could be estimated using local meteorological observations.

### C. Hopfield Model

Hopfield developed another strategy to derive the theoretical formula for hydrostatic delay calculation [36]. In this model, the hydrostatic refractivity profile was assumed to be expressed by the quartic function of height [36]

$$N_h = N_{hs}\left(\frac{H_d - H}{H_d}\right)^4 \tag{23}$$

where $N_{hs}$ is the hydrostatic refractivity at the surface level (unitless) and $H_d$ (unit: meters) represents the equivalent height which is defined as the height above the station where the hydrostatic refractivity is zero. Substituting (23) into (1) and integrating with respect to height, we can obtain

$$\Delta L_h = 10^{-6} \cdot N_{hs} \cdot \frac{H_d}{5}. \tag{24}$$

Hopfield demonstrated that the equivalent height $H_d$ is a linear function of surface temperature $T_s$ [37]. The coefficients between $H_d$ and $T_s$ can be fitted using local meteorological data provided by radiosonde.

Hopfield also assumed that the wet refractivity profile follows the quartic distribution [36], [37]. Following the same approach that is utilized to derive the ZHD, Hopfield got the ZWD expression [36], [37]:

$$\Delta L_w = 10^{-6} \cdot N_{ws} \cdot \frac{H_w}{5} \tag{25}$$

where $N_{ws}$ represents the surface wet refractivity (unitless) and $H_w$ (unit: meters) is the wet equivalent height at which the wet refractivity is zero and the definitions of other variables are the same as before.

### D. Black Model

Based on the Hopfield model, Black developed a more convenient method in the integration of the refractivity. The simple analytical form for the ZHD is [38]

$$\Delta L_h = 2.315 \times 10^{-3} P_s \cdot \frac{T_s - 4.12}{T_s}. \tag{26}$$

Considering the fact that it is difficult to model the variation of atmospheric water vapor with respect to height, Black simply recommended several ZWD correction values under different conditions [38]. He recommended $\Delta L_w = 0.28$ m for summer in tropic or midlatitude regions, $\Delta L_w = 0.20$ m for spring or autumn in midlatitudes, $\Delta L_w = 0.12$ m for winter in maritime midlatitudes, $\Delta L_w = 0.06$ m for winter in continental midlatitudes, and $\Delta L_w = 0.05$ m for polar regions [38].

### E. Goad and Goodman Model

Also, utilizing the Hopfield quartic refractivity model, Goad and Goodman suggested using the length of position vector instead of height [39]. The hydrostatic refractivity model of Hopfield can thus be rewritten as [39]

$$N_h = N_{hs}\left(\frac{r_d - r}{r_d - R_E}\right)^4 \tag{27}$$

where $r_d$ is the distance from the Earth center to the equivalent height of the hydrostatic refractivity (unit: meters), $r$ is the distance from the Earth center to a given height (unit: meters), and $R_E$ is the Earth radius (unit: meters). They gave the final modified Hopfield model in the following form [39]:

$$\Delta L_h = 10^{-6}\cdot N_{hs}\cdot\left[\sum_{k=1}^{9}\frac{\alpha_k}{k}\cdot R^k\right] \tag{28}$$

where $R = r_d - R_E$ and the $\alpha_k$ are represented as

$$\alpha_1 = 1 \quad \alpha_2 = 4a \quad \alpha_3 = 6a^2 + 4b \quad \alpha_4 = 4a(a^2 + 3b)$$
$$\alpha_5 = a^4 + 12a^2b + 6b^2 \quad \alpha_6 = 4ab(a^2 + 3b)$$
$$\alpha_7 = b^2(6a^2 + 4b) \quad \alpha_8 = 4ab^3 \quad \alpha_9 = b^4$$

where $a = -(\sin ele/H_d)$, $b = -(\cos^2 ele/2H_dR_E)$, $ele$ (unit: radians) is the elevation angle of the ray path, and $H_d$ has been defined in (23).

Following the procedure in deriving the ZHD model, Goad and Goodman derived the ZWD model [39]:

$$\Delta L_w = 10^{-6}\cdot N_{ws}\cdot\left[\sum_{k=1}^{9}\frac{\alpha_k}{k}\cdot R^k\right] \tag{29}$$

where $R = r_w - R_E\cdot r_w$ (unit: meters) is the distance from the Earth center to the equivalent height of the wet refractivity. The other variables are the same as those in (28), except replacing $H_d$ with $H_w$ in the calculation of $a$ and $b$.

### F. UNB3 and EGNOS Models

In the ZHD and ZWD calculations using the models described previously, the surface meteorological observation data such as pressure and temperature are required. In the UNB3 model, empirical meteorological data are used, and they are predicted from the U.S. Standard Atmosphere Supplements, 1966 [40], [41]. The ZHD is calculated as [42]

$$\Delta L_h = z_d\cdot\left[1 - \frac{\alpha\cdot H}{T_0}\right]^{\frac{g}{R_d\cdot\alpha}} \tag{30}$$

where $\alpha$ represents the temperature lapse rate (unit: kelvin per kilometer), $H$ is the height of the station above mean sea level (unit: meters), $T_0$ is the temperature at mean sea level (unit: kelvin), $g$ is the surface acceleration of gravity (unit: meters per square second), $R_d$ has been defined in (4), and $z_d$ is the ZHD at mean sea level (unit: meters) and is computed by [42]

$$z_d = \frac{10^{-6}k_1\cdot R_d\cdot p_0}{g_m} \tag{31}$$

TABLE II
ANNUAL AVERAGE VALUES AND SEASONAL VARIATION VALUES OF THE METEOROLOGICAL PARAMETERS USED IN THE UNB3/EGNOS MODEL

| Average | | | | | | |
|---|---|---|---|---|---|---|
| Latitude (°) | $P_0$ (hPa) | $T_0$ (K) | $e_0$ (hPa) | $\alpha$ (K/km) | $\lambda$ | $RH$ (%) |
| $\leq 15$ | 1013.25 | 299.65 | 26.31 | 6.30 | 2.77 | 75.0 |
| 30 | 1017.25 | 294.15 | 21.79 | 6.05 | 3.15 | 80.0 |
| 45 | 1015.75 | 283.15 | 11.66 | 5.58 | 2.57 | 76.0 |
| 60 | 1011.75 | 272.15 | 6.78 | 5.39 | 1.81 | 77.5 |
| $\geq 75$ | 1013.00 | 263.65 | 4.11 | 4.53 | 1.55 | 82.5 |
| Seasonal Variation | | | | | | |
| Latitude (°) | $\Delta P_0$ (hPa) | $\Delta T_0$ (K) | $\Delta e_0$ (hPa) | $\Delta\alpha$ (K/km) | $\Delta\lambda$ | $\Delta RH$ (%) |
| $\leq 15$ | 0.00 | 0.00 | 0.00 | 0.00 | 0.00 | 0.0 |
| 30 | -3.75 | 7.00 | 8.85 | 0.25 | 0.33 | 0.0 |
| 45 | -2.25 | 11.00 | 7.24 | 0.32 | 0.46 | -1.0 |
| 60 | -1.75 | 15.00 | 5.36 | 0.81 | 0.74 | -2.5 |
| $\geq 75$ | -0.50 | 14.50 | 3.39 | 0.62 | 0.30 | 2.5 |

where $k_1$ has been defined in (2), $p_0$ is the atmospheric pressure at mean sea level (unit: hectopascals), and $g_m$ can be computed from (12). For a certain station and specified date, $p_0$, $T_0$, and $\alpha$ can be computed using the following formula:

$$\xi(\phi, D) = \xi_0(\phi) - \Delta\xi(\phi)\cdot\cos\left[\frac{2\pi\cdot(D - D_{\min})}{365.25}\right] \tag{32}$$

where $\xi_0$ and $\Delta\xi$ are the annual average and seasonal variations, respectively, for a certain parameter at a station with latitude $\phi$, $D$ is the day-of-year for which the computation is performed, $D_{\min} = 28$ in the Northern Hemisphere, and $D_{\min} = 211$ in the Southern Hemisphere. The annual average values and seasonal variations for the meteorological parameters were derived from North American meteorological data, and they are given in Table II. The expression of the EGNOS ZHD model is almost identical to the UNB3 ZHD model. The only slight difference between the two models is that $g$ and $g_m$ are set as constant values in the EGNOS model, and their values are 9.80665 and 9.784 m $\cdot$ s$^{-2}$, respectively [42].

In the UNB3 model, the ZWD is computed using [42]

$$\Delta L_w = z_w\cdot\left[1 - \frac{\alpha\cdot H}{T_0}\right]^{\frac{(\lambda+1)\cdot g}{R_d\cdot\alpha} - 1} \tag{33}$$

where $\lambda$ is the water vapor lapse rate (unitless), $z_w$ is the ZWD at mean sea level (unit: meters), and it is calculated using the following formula:

$$z_w = \frac{10^{-6}\left(T_m k_2' + k_3\right)R_d}{g_m(\lambda + 1) - \beta\cdot R_d}\cdot\frac{e_0}{T_0} \tag{34}$$

where $k_2' = k_2 - k_1\cdot R_d/R_w$ and $T_m$ is the mean temperature (unit: kelvin) that can be calculated from

$$T_m = T_s\cdot\left(1 - \frac{\alpha\cdot R_d}{(\lambda + 1)\cdot g_m}\right). \tag{35}$$

The parameters $T_0$, $\beta$, and $\lambda$ can also be computed using the expression in (32). The annual average values and seasonal variations for these parameters are given in Table II. In the original version of UNB3, water vapor pressure $e_0$ is directly

obtained using the same method as $p_0$ from the look-up Table II. Later, Leandro *et al.* found that $RH$ calculated from $e_0$ is greater than 100% in some cases [43]. Thus, they modified the UNB3 model to avoid the problematic values of $RH$. In the modified model, $RH$ is first predicted from the look-up table. Then, water vapor pressure $e_0$ is computed from (3). For the EGNOS ZWD model, its expression is also almost identical to UNB3, except that $T_m k_2' + k_3$ is simply set as 382 000 $K^2$/hPa and $e_0$ is directly obtained from Table II [42].

### G. GPT2 Model

Based on the spherical harmonics, Boehm *et al.* developed an empirical global pressure and temperature model (GPT) that can provide pressure and temperature at any location in the vicinity of the Earth's surface [44]. Lagler *et al.* improved this model, and a new version called GPT2 is now available [45]. Besides the pressure and temperature, the refined GPT2 model also outputs parameters such as water vapor pressure, water vapor lapse rate, and temperature lapse rate. The GPT2 model can be accessible at the International Earth Rotation and Reference Systems Service (IERS) Conventions Product Center (http://62.161.69.131/iers/convupdt/convupdt.html).

### H. ECMWF Model

The European Centre for Medium-Range Weather Forecasts (ECMWF) provides a set of global analysis and reanalysis data of the atmosphere. Based on atmospheric physical models, meteorological data from *in situ* observations (e.g., surface weather stations, ships, buoys, radiosonde stations, and aircraft) and remote sensing observations are assimilated into the atmospheric models to generate the analysis and reanalysis data (http://old.ecmwf.int/products/forecasts/guide/user_guide.pdf). In this paper, we use the latest global atmospheric reanalysis product ERA-Interim [46] to produce the ZHD and ZWD. The data have a horizontal resolution of $0.5^\circ \times 0.5^\circ$ and a vertical resolution of 37 isobaric levels extending from 1000 to 1 hPa. For a certain site, meteorological parameters are derived using bilinear interpolation of the ECMWF data at four surrounding grid points. Finally, ZHD and ZWD can be calculated using (8) and (9), respectively.

### I. Berman Models

In Sections III-A–H, formulas for the estimation of both ZHD and ZWD have been developed in each model. From this Section III-I on, only the formula for ZWD calculation is developed. Under the assumption of linear temperature lapse, constant relative humidity, and wet refractivity reducing to zero at the tropopause, Berman obtained the "Berman 70" ZWD model [47]

$$\Delta L_w = \frac{373}{\alpha(B - A \cdot C)} \cdot \left(1 - \frac{C}{T_s}\right)^2 \cdot e_s \tag{36}$$

where $A$, $B$, and $C$ are hygrometric constants, and their values are 17.1485, 4684.1, and 38.45, respectively. Berman also derived other three improved models, i.e., "Berman 74," "Berman (TMOD)," and "Berman (D/N)" models. The general expression of these models is written as

$$\Delta L_w = 10.946 \cdot K \cdot \frac{e_s}{T_s}. \tag{37}$$

In the "Berman 74" model, $K$ is set as 0.3224, and in the "Berman (TMOD)" model, $K$ is set as 0.3281. By analyzing the meteorological parameter profiles separately for day and night cases, Berman developed a "Berman (D/N)" model, in which $K = 0.2896$ for the day case and $K = 0.3773$ for the night case.

### J. Callahan Model

Callahan assumed that the water vapor pressure distribution could be empirically expressed in the following form [48]:

$$e = e_s \cdot \exp(-2.88 \times 10^{-4} \cdot H - 4.8 \times 10^{-8} \cdot H^2) \tag{38}$$

where $e_s$ is the surface water vapor pressure and $H$ is the height above the ground surface level (unit: meters). A complete derivation of the Callahan model is very complicated. By using a set of nominal values, the simplified final form is given as follows [9]:

$$\Delta L_w = \frac{1\,035 \cdot e_s}{T_s^2}. \tag{39}$$

### K. Chao Model

The ZWD model developed by Chao assumes that water vapor obeys the hydrostatic law and adopts the adiabatic approximation to the water vapor [49]. The model's final form is given as

$$\Delta L_w = 1.63 \cdot \frac{e_s^{1.23}}{T_s^2} + 2.05 \cdot \alpha \cdot \frac{e_s^{1.46}}{T_s^3}. \tag{40}$$

In this model, the $\Delta L_w$ is not very sensitive to the temperature lapse rate $\alpha$. The use of a mean value of $\alpha$ (e.g., 6.5 K/km) can lead to an adequate accuracy for the model. To enhance the model's performance, $\alpha$ could be estimated using local meteorological observations.

### L. Ifadis Model

Ifadis developed a global ZWD model considering a linear relationship between the ZWD and the surface meteorological data [9]. The formula of this model is given as follows [9]:

$$\Delta L_w = 0.00554 - 0.880 \times 10^{-4} \cdot (P_s - 1\,000.0) + 0.272 \times 10^{-4} \cdot e_s + 2.771 \cdot \frac{e_s}{T_s} \tag{41}$$

where $P_s$, $e_s$, and $T_s$ are the atmospheric pressure, water vapor pressure, and temperature at the surface, respectively.

### M. Askne and Nordius Model

Under the assumption that water vapor pressure decreases with height in the same way as the total pressure, the water vapor pressure can be expressed in the form [27]

$$e = e_s \cdot \left(\frac{P}{P_s}\right)^{\omega+1} \tag{42}$$

where $e_s$ and $P_s$ are the water vapor pressure and atmospheric pressure at the surface, respectively, $P$ is the atmospheric pressure, and $\omega$ is a parameter associated with seasonal and latitudinal variations (unitless). $\omega$ should be determined using local atmospheric profiles. Substituting (42) into the last term of (7) and after some integrals and calculations, the following is obtained:

$$\Delta L_w = 10^{-6} \cdot (k_2' + k_3/T_m) \cdot \frac{R_d}{(\omega+1) \cdot g_m} \cdot e_s \tag{43}$$

where $T_m$ is calculated by

$$T_m = T_s \cdot \left(1 - \frac{\alpha \cdot R_d}{(\omega+1) \cdot g_m}\right). \tag{44}$$

## IV. Radiosonde Measurement and Its Accuracy

### A. Data Description

Based on the balloonborne platform, a radiosonde can directly measure the meteorological parameters such as atmospheric pressure, temperature, and relative humidity at different altitudes from the ground surface to a height of up to over 30 km [50]. Thus, according to (5) and (6), the hydrostatic and wet refractivity profiles can be determined. Finally, the zenith hydrostatic and wet delays could be easily calculated according to (8) and (9). Due to the high accuracy of radiosonde data, radiosonde-derived results are usually adopted as reference for other instruments/models [51]. In this paper, the zenith hydrostatic and wet delays derived from radiosonde are also adopted as reference data to assess the accuracy of each tropospheric delay model. It should be noted that the radiosonde balloon usually could not reach the height where air pressure is zero. This can usually result in an error varying from 2 to 6 cm for the ZHD measurement [35]. For some cases, if the radiosonde balloons fail to reach a high enough altitude, it can cause an error up to 1 m [35]. Therefore, to ensure the quality of ZHD derived from radiosonde, only radiosonde data that contain complete meteorological parameter profiles up to the height with a pressure equal to or less than 30 hPa are used in our study [37]. In order to compensate the hydrostatic delay between 30 hPa (or less than 30 hPa) and zero pressure that cannot be measured by radiosonde, we use (14) to calculate a small correction. This correction is added to the hydrostatic delay computed from (8) [35]. In this way, the calculated ZHD approaches the true value as much as possible [35].

In order to achieve a statistically meaningful conclusion, a large volume of radiosonde observations collected from a total of 92 stations in China over a 10-year period from 2003 to 2012 is utilized to evaluate the performances of different tropospheric delay models. Fig. 1 presents the geographic distribution of

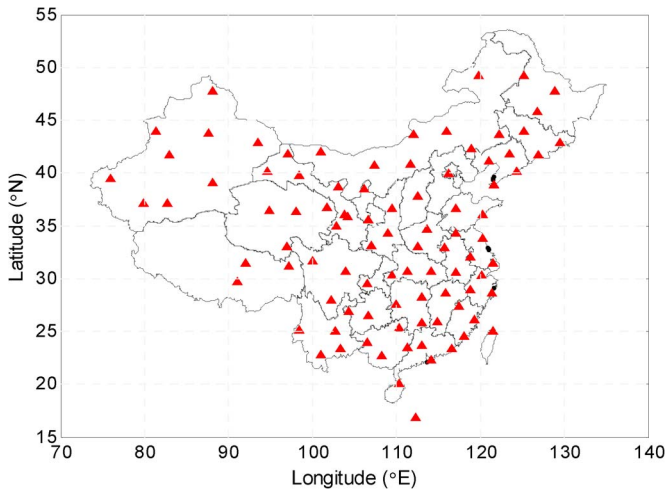


Fig. 1. Geographic distribution of 92 radiosonde stations (red solid triangles) in China.

92 radiosonde stations. Before 2006, 80 radiosonde stations were equipped with CHINA GZZ-2 sensors, 10 radiosonde stations were equipped with CHINA GTS1 sensors, and 2 radiosonde stations were equipped with Vaisala RS80 sensors. After 2006, 52 radiosonde stations equipped with CHINA GZZ-2 were replaced by CHINA GTS1. In addition, the two radiosonde stations equipped with Vaisala RS80 were replaced by Vaisala RS92. Thus, after 2006, there are 28 radiosonde stations equipped with CHINA GZZ-2, and the number of radiosonde stations equipped with CHINA GTS1 increases to 62. Radiosonde instruments of the rest two stations are Vaisala RS92. Several studies showed that the Chinese-made radiosonde CHINA GZZ-2 and CHINA GTS1 can achieve a comparable performance with the Vaisala radiosonde [52]–[54].

### B. Accuracy of the Radiosonde-Derived Zenith Hydrostatic and Wet Delays

In order to evaluate the accuracy of the ZHD derived from the radiosonde, we first differentiate (8)

$$d_{\Delta L_h} = 10^{-6}\left(\sum A_{i+1} d_{N_{h_{i+1}}} - \sum A_i d_{N_{h_i}}\right) \tag{45}$$

where $A_{i+1}$ and $A_i$ are defined as

$$A_{i+1} = (H_i - H_{i+1}) \cdot \frac{\left(\ln N_{h_i} - \ln N_{h_{i+1}} + \frac{N_{h_{i+1}} - N_{h_i}}{N_{h_{i+1}}}\right)}{\left(\ln N_{h_i} - \ln N_{h_{i+1}}\right)^2} \tag{46}$$

$$A_i = (H_i - H_{i+1}) \cdot \frac{\left(\ln N_{h_i} - \ln N_{h_{i+1}} + \frac{N_{h_{i+1}} - N_{h_i}}{N_{h_i}}\right)}{\left(\ln N_{h_i} - \ln N_{h_{i+1}}\right)^2}. \tag{47}$$

Then, (5) can be differentiated as

$$d_{N_h} = \frac{k_1}{T} d_{P_d} + \frac{k_1 \cdot R_d}{T \cdot R_w} d_e - k_1 \cdot \left(\frac{P_d}{T^2} + \frac{e \cdot R_d}{T^2 \cdot R_w}\right) d_T \tag{48}$$

where $d_e$ can be derived from (3)

$$d_e = Q \cdot d_P + R \cdot d_T + S \cdot d_{RH} \tag{49}$$

where $Q$, $R$, and $S$ represent

$$\begin{aligned} Q &= 21.147866 \times 10^{-6} \cdot RH \cdot e^{\theta} \\ R &= 6.1121 \times RH(1.0007 + 3.46 \times 10^{-6} \cdot P) \cdot e^{\theta} \\ &\quad \cdot \frac{18.729 - 2 \times (T - 273.15)/227.3 - \theta}{T - 15.28} \\ S &= 6.1121 \times (1.0007 + 3.46 \times 10^{-6} \cdot P) \cdot e^{\theta} \\ \theta &= \frac{[18.729 - (T - 273.15)/227.3] \cdot (T - 273.15)}{T - 15.28}. \end{aligned}$$

Considering the total atmospheric pressure $P$ equal to the sum of $P_d$ and $e$, we rewrote (48) as

$$\begin{aligned} d_{N_h} = &\left[\frac{k_1}{T} + \left(\frac{k_1 \cdot R_d}{T \cdot R_w} - \frac{k_1}{T}\right) \cdot Q\right] \cdot d_P \\ &+ \left[\left(\frac{k_1 \cdot R_d}{T \cdot R_w} - \frac{k_1}{T}\right) \cdot R - k_1 \left(\frac{P_d}{T^2} - \frac{e \cdot R_d}{T^2 \cdot R_w}\right)\right] \\ &\cdot d_T + \left(\frac{k_1 \cdot R_d}{T \cdot R_w} - \frac{k_1}{T}\right) \cdot S \cdot d_{RH}. \end{aligned} \tag{50}$$

Substituting (50) into (45) and assuming that the measurements of pressure, temperature, and relative humidity are uncorrelated, we can derive the uncertainty of ZHD, denoted as $\sigma_{\Delta L_h}$, by utilizing the error propagation law

$$\sigma_{\Delta L_h} = 10^{-6} \cdot \sqrt{B_1 \cdot \sigma_P^2 + B_2 \cdot \sigma_T^2 + B_3 \cdot \sigma_{RH}^2} \tag{51}$$

where $\sigma_P$, $\sigma_T$, and $\sigma_{RH}$ are the uncertainties of the total pressure, temperature, and relative humidity measurements, respectively. In addition, the coefficients $B_1$, $B_2$, and $B_3$ are defined as

$$\begin{aligned} B_1 = \sum \Bigg\{ &A_{i+1}^2 \cdot \left[\frac{k_1}{T_{i+1}} + \left(\frac{k_1 \cdot R_d}{T_{i+1} \cdot R_w} - \frac{k_1}{T_{i+1}}\right) \cdot Q_{i+1}\right]^2 \\ &+ A_i^2 \cdot \left[\frac{k_1}{T_i} + \left(\frac{k_1 \cdot R_d}{T_i \cdot R_w} - \frac{k_1}{T_i}\right) \cdot Q_i\right]^2 \Bigg\} \\ B_2 = \sum \Bigg\{ &A_{i+1}^2 \cdot \left[\left(\frac{k_1 \cdot R_d}{T_{i+1} \cdot R_w} - \frac{k_1}{T_{i+1}}\right) \cdot R_{i+1} \right. \\ &\left. - k_1 \cdot \left(\frac{P_{d_{i+1}}}{T_{i+1}^2} + \frac{R_d \cdot e_{i+1}}{R_w \cdot T_{i+1}^2}\right)\right]^2 + A_i^2 \\ &\cdot \left[\left(\frac{k_1 \cdot R_d}{T_i \cdot R_w} - \frac{k_1}{T_i}\right) \cdot R_i - k_1 \cdot \left(\frac{P_{d_i}}{T_i^2} + \frac{R_d \cdot e_i}{R_w \cdot T_i^2}\right)\right]^2 \Bigg\} \\ B_3 = \sum \Bigg\{ &(A_{i+1} \cdot S_{i+1})^2 \cdot \left(\frac{k_1 \cdot R_d}{T_{i+1} \cdot R_w} - \frac{k_1}{T_{i+1}}\right)^2 \\ &+ (A_i \cdot S_i)^2 \cdot \left(\frac{k_1 \cdot R_d}{T_i \cdot R_w} - \frac{k_1}{T_i}\right)^2 \Bigg\}. \end{aligned}$$

TABLE III
UNCERTAINTY VALUES ESTIMATED FROM THE RADIOSONDE MEASUREMENTS

| | Maximum | Minimum | Mean |
|---|---|---|---|
| $B_1$ | $5.51\times10^{6}$ | $7.47\times10^{5}$ | $3.19\times10^{6}$ |
| $B_2$ | $6.66\times10^{7}$ | $8.42\times10^{5}$ | $1.02\times10^{7}$ |
| $B_3$ | $1.40\times10^{7}$ | $7.93\times10^{3}$ | $3.09\times10^{6}$ |
| $D_1$ | $1.66\times10^{-1}$ | $2.13\times10^{-5}$ | $2.48\times10^{-2}$ |
| $D_2$ | $5.70\times10^{7}$ | $1.00\times10^{4}$ | $7.62\times10^{6}$ |
| $D_3$ | $2.83\times10^{10}$ | $1.89\times10^{7}$ | $6.96\times10^{9}$ |
| $\sigma_{\Delta L_h}$ | 4.71 mm | 0.98 mm | 2.40 mm |
| $\sigma_{\Delta L_w}$ | 9.22 mm | 0.22 mm | 4.39 mm |

Following the same procedure, we can derive the uncertainty of the ZWD, denoted as $\sigma_{\Delta L_w}$

$$\sigma_{\Delta L_w} = 10^{-6} \cdot \sqrt{D_1 \cdot \sigma_P^2 + D_2 \cdot \sigma_T^2 + D_3 \cdot \sigma_{RH}^2} \tag{52}$$

where

$$\begin{aligned} D_1 = \sum \Bigg[ &(C_{i+1} \cdot Q_{i+1})^2 \cdot \left(\frac{k_2'}{T_{i+1}} + \frac{k_3}{T_{i+1}^2}\right)^2 \\ &+ (C_i \cdot Q_i)^2 \cdot \left(\frac{k_2'}{T_i} + \frac{k_3}{T_i^2}\right)^2 \Bigg] \\ D_2 = \sum \Bigg[ &C_{i+1}^2 \cdot \left[\left(\frac{k_2'}{T_{i+1}} + \frac{k_3}{T_{i+1}^2}\right) \cdot R_{i+1} \right. \\ &\left. - \left(\frac{k_2' \cdot e_{i+1}}{T_{i+1}^2} + \frac{2 \cdot k_3 \cdot e_{i+1}}{T_{i+1}^3}\right)\right]^2 + C_i^2 \\ &\cdot \left[\left(\frac{k_2'}{T_i} + \frac{k_3}{T_i^2}\right) \cdot R_i - \left(\frac{k_2' \cdot e_i}{T_i^2} + \frac{2 \cdot k_3 \cdot e_i}{T_i^3}\right)\right]^2 \Bigg] \\ D_3 = \sum \Bigg[ &(C_{i+1} \cdot S_{i+1})^2 \cdot \left(\frac{k_2'}{T_{i+1}} + \frac{k_3}{T_{i+1}}\right)^2 \\ &+ (C_i \cdot S_i)^2 \cdot \left(\frac{k_2'}{T_i} + \frac{k_3}{T_i^2}\right)^2 \Bigg] \end{aligned}$$

$$C_{i+1} = (H_i - H_{i+1}) \cdot \frac{\left(\ln N_{w_i} - \ln N_{w_{i+1}} + \frac{N_{w_{i+1}} - N_{w_i}}{N_{w_{i+1}}}\right)}{\left(\ln N_{w_i} - \ln N_{w_{i+1}}\right)^2}$$

$$C_i = (H_i - H_{i+1}) \cdot \frac{\left(\ln N_{w_i} - \ln N_{w_{i+1}} + \frac{N_{w_{i+1}} - N_{w_i}}{N_{w_i}}\right)}{\left(\ln N_{w_i} - \ln N_{w_{i+1}}\right)^2}.$$

By utilizing the 10-year radiosonde data of the 92 stations, we calculated the empirical values of $B_1$, $B_2$, $B_3$, $D_1$, $D_2$, and $D_3$ for each station. Here, we only give their maximum, minimum, and mean values in Table III. According to [55], the Chinese-made radiosonde can fully meet the accuracy requirements for upper air meteorological measurements in the Commission for Instruments and Methods of Observations (CIMO) Guide [50]. Thus, we used the standard errors established in the CIMO Guide to derive the uncertainties of ZHD and ZWD. The specified pressure, temperature, and $RH$ accuracies for radiosonde instrumentation are $\sigma_P = 1$ hPa, $\sigma_T = 0.5$ K, and $\sigma_{RH} = 0.05$, respectively. Substituting these values and those

TABLE IV
ZHD AND ZWD MODELS AND THEIR ABBREVIATION CODES AND INPUT PARAMETERS

| No. | Model Name | ZHD Model Code (input parameters) | ZWD Model Code (input parameters) |
|---|---|---|---|
| 1 | Askne and Nordius | -- | AN_ZW ($e_s, T_s, \omega, \alpha$) |
| 2 | Baby semi-empirical | -- | BAS_ZW ($T_s, RH, v, \gamma$) |
| 3 | Baby theoretical | BA_ZH ($P_S, T_s, \alpha$) | BA_ZW ($T_s, RH, \alpha, H_w$) |
| 4 | Berman70 | -- | B70_ZW ($e_s, T_s, \alpha$) |
| 5 | Berman74 | -- | B74_ZW ($e_s, T_s$) |
| 6 | Berman D/N | -- | BDN_ZW ($e_s, T_s$) |
| 7 | Berman TMOD | -- | BTM_ZW ($e_s, T_s$) |
| 8 | Black | BL_ZH ($P_s, T_s$) | BL_ZW (--) |
| 9 | Callahan | -- | CA_ZW ($e_s, T_s$) |
| 10 | Chao | -- | CH_ZW ($e_s, T_s, \alpha$) |
| 11 | ECMWF | EC_ZH (--) | EC_ZW (--) |
| 12 | EGNOS | EG_ZH (--) | EG_ZW (--) |
| 13 | Goad and Goodman | GG_ZH ($P_s, T_s, H_d$) | GG_ZW ($e_s, T_s, H_w$) |
| 14 | GPT2 | GP_ZH (--) | GP_ZW (--) |
| 15 | Hopfield | HO_ZH ($P_s, T_s, H_d$) | HO_ZW ($e_s, T_s, H_w$) |
| 16 | Ifadis | -- | IF_ZW ($P_s, e_s, T_s$) |
| 17 | Saastamoinen | SA_ZH ($P_s$) | SA_ZW ($e_s, T_s$) |
| 18 | UNB3 | UN_ZH (--) | UN_ZW (--) |

in Table III into (51) and (52), the corresponding $\sigma_{\Delta L_h}$ and $\sigma_{\Delta L_w}$ are obtained and given in the last two rows of Table III. Results show that the mean accuracies (standard deviation) of ZHD and ZWD derived from the radiosonde are 2.4 and 4.4 mm, respectively. Thus, radiosonde data can be adopted as an accuracy standard to evaluate the performances of the tropospheric delay models.

## V. TROPOSPHERIC MODEL ASSESSMENT

In the model evaluation, all of the models are used to calculate the tropospheric hydrostatic and wet delays for the geographic locations of each radiosonde site (site's latitude, longitude, and height are known). This ensures that the delays observed from radiosonde and calculated from the models can be directly compared. In the model computation, all of the models, except UNB3, EGNOS, GPT2, and ECMWF, need surface meteorological parameters, and they are extracted from radiosonde observations. In order to evaluate the GPT2 model, we exploit the Baby ZHD model and Askne ZWD model to calculate the ZHD and ZWD, respectively, using the empirical meteorological parameters provided by the GPT2 model. This is because in Section V-A we find that the Baby model is the most accurate one among all of the ZHD models if their meteorological parameters can be obtained from the GPT2. In the same way, we choose the Askne ZWD model to compute the ZWD by using meteorological parameters from the GPT2 model. For the sake of convenience, each model is abbreviated with a code as listed Table IV. In addition, we may notice that the calculation of some models needs some other parameters in addition to surface observations (see Table IV). The parameters in the hydrostatic models include $\alpha$ (in BA_ZH) and $H_d$ (e.g., HO_ZH and GG_ZH), and the parameters in the wet models include $H_w$ (in HO_ZW, GG_ZW, and BA_ZW), $\alpha$ (in AN_ZW, BA_ZW, B70_ZW, and CH_ZW), $\omega$ (in AN_ZW), $v$, and $\gamma$ (in BAS_ZW). In this paper, the values of all of these parameters are fitted from radiosonde observations for each site in order to enhance the modeling performance. Specifically, according to each model's expression, radiosonde-derived ZHDs/ZWDs are exploited to estimate the parameters in this model by performing a least-squares fitting method. The accuracies of the models will be assessed in terms of mean bias, standard deviation (STD), and root-mean-square (rms) error against the radiosonde-derived hydrostatic and wet delays.

TABLE V
STATISTICAL RESULTS OF THE DIFFERENCES BETWEEN ZHD DERIVED FROM EMPIRICAL MODELS AND ZHD FROM 10 YEARS (2003–2012) OF OBSERVATIONS AT 92 RADIOSONDE STATIONS (UNIT: MILLIMETERS)

| Model | Mean | STD | RMS |
|---|---|---|---|
| BA_ZH | -1.3 | 5.8 | 6.0 |
| BL_ZH | -5.1 | 6.0 | 7.8 |
| EC_ZH | 0.9 | 2.6 | 2.8 |
| EG_ZH | -5.3 | 17.1 | 17.9 |
| GG_ZH | -0.7 | 6.0 | 6.1 |
| GP_ZH | 1.4 | 11.5 | 11.6 |
| HO_ZH | -0.7 | 6.0 | 6.1 |
| SA_ZH | -6.0 | 5.9 | 8.4 |
| UN_ZH | -0.8 | 17.4 | 19.1 |

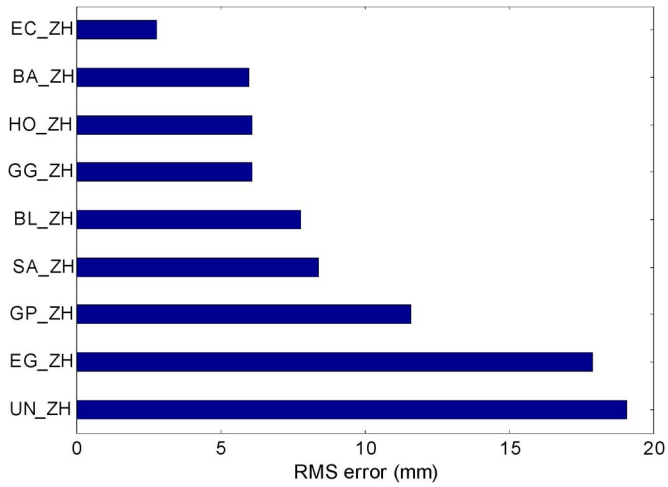


Fig. 2. Ranking of the ZHD models by the size of the rms errors.

### A. Assessment of ZHD Models With Radiosonde

*1) Overall Performance of the ZHD Models:* Using the measurements recorded during the 10-year period at 92 radiosonde stations as references, the overall performances of the 9 ZHD models are evaluated. Table V lists the means, STD, and rms errors of the differences between ZHDs derived from radiosonde measurements and empirical models. Fig. 2 shows the ranking of the ZHD models by the size of the rms errors. As shown in Table V and Fig. 2, we can find that EC_ZH achieves the best performance with an accuracy of 2.8 mm and UN_ZH performs the worst with an rms error of 19.1 mm. It is not surprising that the EC_ZH model has a good agreement with the radiosonde data since the radiosonde observations have also been employed to generate the ECMWF reanalysis data. BA_ZH, HO_ZH, and GG_ZH have very similar performances, although they are not as good as EC_ZH. In addition, we notice that HO_ZH and GG_ZH actually have identical performances. This is because GG_ZH is a modified model from HO_ZH, and its expression

TABLE VI
SEASONAL STATISTICS OF DIFFERENCES BETWEEN ZHD DERIVED FROM EMPIRICAL MODELS AND ZHD FROM 10 YEARS (2003–2012) OF OBSERVATIONS AT 92 RADIOSONDE STATIONS (UNIT: MILLIMETERS)

| Model | | Spring | Summer | Autumn | Winter |
|---|---|---|---|---|---|
| BA_ZH | Mean | -1.4 | -1.9 | -1.3 | -0.6 |
| | STD | 5.8 | 5.8 | 5.9 | 5.8 |
| | RMS | 6.0 | 6.1 | 6.1 | 5.8 |
| BL_ZH | Mean | -5.2 | -6.8 | -5.2 | -3.0 |
| | STD | 5.8 | 5.7 | 6.0 | 5.8 |
| | RMS | 7.8 | 8.9 | 8.0 | 6.5 |
| EC_ZH | Mean | 0.7 | 1.2 | 0.7 | 1.2 |
| | STD | 2.6 | 2.4 | 2.4 | 3.0 |
| | RMS | 2.7 | 2.6 | 2.6 | 3.2 |
| EG_ZH | Mean | -8.7 | -21.3 | -0.1 | 8.4 |
| | STD | 14.6 | 9.6 | 12.7 | 15.1 |
| | RMS | 17.0 | 23.3 | 12.7 | 17.2 |
| GG_ZH | Mean | -2.3 | -1.9 | -1.3 | -1.0 |
| | STD | 5.8 | 5.6 | 5.6 | 6.3 |
| | RMS | 6.3 | 5.9 | 5.7 | 6.4 |
| GP_ZH | Mean | 1.2 | 0.2 | 1.3 | 2.9 |
| | STD | 12.6 | 9.0 | 10.5 | 13.3 |
| | RMS | 12.7 | 9.0 | 10.6 | 13.6 |
| HO_ZH | Mean | -2.3 | -1.9 | -1.3 | -1.0 |
| | STD | 5.8 | 5.6 | 5.6 | 6.3 |
| | RMS | 6.3 | 5.9 | 5.7 | 6.4 |
| SA_ZH | Mean | -6.1 | -6.5 | -6.1 | -5.3 |
| | STD | 5.8 | 5.8 | 6.0 | 5.8 |
| | RMS | 8.4 | 8.8 | 8.5 | 7.9 |
| UN_ZH | Mean | -11.3 | -23.8 | -2.7 | 5.7 |
| | STD | 14.9 | 9.8 | 13.2 | 15.7 |
| | RMS | 18.7 | 25.8 | 13.5 | 16.7 |

is the same as HO_ZH in the zenith mode. The BL_ZH and SA_ZH models also show good performances with an accuracy of about 8 mm. It is interesting to see that GP_ZH achieved an accuracy of 11.6 mm. Also, using the empirical meteorological parameters, EG_ZH and UN_ZH show similar performances, with rms errors of 17.9 and 19.1 mm, respectively. Therefore, it is better to employ GP_ZH rather than EG_ZH or UN_ZH to provide the ZHD corrections when surface meteorological parameters are unavailable or a quick tropospheric correction with modest precision is needed.

*2) Seasonal Performance of the ZHD Models:* Table VI presents the performances of the nine ZHD models for different seasons. For the best accuracy model EC_ZH, we can notice that there are no significant differences among the four seasons. Similarly, BA_ZH, BL_ZH, GG_ZH, GP_ZH, HO_ZH, and SA_ZH are very consistent over the seasons, and no significant variations have been observed in their rms errors from spring to winter. However, the EG_ZH and UN_ZH show significant seasonal variations. In terms of temporal performance over seasons, it can be seen that the EC_ZH is the best model, which is consistent with the results in Fig. 2.

*3) Assessment of the ZHD Models at Different Latitudinal Regions:* In addition to the overall and seasonal performances, we also investigate the performances of the ZHD models at different latitudinal regions in China. China covers the region from 15° N to 55° N in latitude. The ZHD model performance in four regions 15–25° N, 25–35° N, 35–45° N, and 45–55° N are studied. As shown in Table VII, the performances of the models vary with latitudes, and EC_ZH performs best in all of the four regions. For BA_ZH, BL_ZH, GG_ZH, HO_ZH, and SA_ZH, their accuracies in 35–55° N are higher than those in 15–35° N. However, for the EG_ZH and GP_ZH, their accuracies in 35–55° N are lower than in 15–35° N latitude zones. It is worthwhile to note that GP_ZH also utilizes the BA_ZH to compute the ZHD, but they show opposite performances. In other words, this perhaps reveals that the GPT2 can provide better predictions of the meteorological parameters in low-latitude regions in China.

TABLE VII
STATISTICS OF DIFFERENCES BETWEEN ZHD DERIVED FROM EMPIRICAL MODELS AND ZHD FROM 10 YEARS (2003–2012) OF OBSERVATIONS AT 92 RADIOSONDE STATIONS AT DIFFERENT LATITUDINAL REGIONS (UNIT: MILLIMETERS)

| Model | | Latitudinal Regions (°N) | | | |
|---|---|---|---|---|---|
| | | 15~25 | 25~35 | 35~45 | 45~55 |
| BA_ZH | Mean | -3.9 | -2.2 | -1.0 | 2.1 |
| | STD | 3.3 | 5.7 | 3.3 | 2.6 |
| | RMS | 5.1 | 6.1 | 3.4 | 3.4 |
| BL_ZH | Mean | -7.1 | -5.6 | -4.8 | -3.4 |
| | STD | 3.5 | 5.8 | 4.3 | 3.8 |
| | RMS | 7.9 | 8.1 | 6.4 | 5.1 |
| EC_ZH | Mean | 0.4 | 0.7 | 1.4 | 1.3 |
| | STD | 2.1 | 2.6 | 2.7 | 2.5 |
| | RMS | 2.1 | 2.7 | 3.0 | 2.8 |
| EG_ZH | Mean | -10.7 | -7.2 | -1.8 | -2.9 |
| | STD | 12.9 | 16.0 | 17.8 | 20.3 |
| | RMS | 16.7 | 17.6 | 17.9 | 20.5 |
| GG_ZH | Mean | 0.2 | -1.0 | -0.8 | -1.2 |
| | STD | 6.8 | 6.0 | 5.9 | 4.3 |
| | RMS | 6.9 | 6.1 | 5.9 | 4.4 |
| GP_ZH | Mean | -0.9 | -0.1 | 4.0 | 1.1 |
| | STD | 8.6 | 10.5 | 11.9 | 14.3 |
| | RMS | 8.6 | 10.5 | 12.6 | 14.4 |
| HO_ZH | Mean | 0.2 | -1.0 | -0.8 | -1.2 |
| | STD | 6.8 | 6.0 | 5.9 | 4.3 |
| | RMS | 6.9 | 6.1 | 5.9 | 4.4 |
| SA_ZH | Mean | -8.8 | -6.9 | -5.5 | -2.8 |
| | STD | 3.3 | 5.7 | 3.4 | 2.5 |
| | RMS | 9.4 | 9.0 | 6.4 | 3.8 |
| UN_ZH | Mean | -15.2 | -10.6 | -3.5 | -2.5 |
| | STD | 12.9 | 16.1 | 17.8 | 20.3 |
| | RMS | 19.9 | 19.3 | 18.1 | 20.5 |

TABLE VIII
STATISTICAL RESULTS OF DIFFERENCES BETWEEN ZWD DERIVED FROM EMPIRICAL MODELS AND ZWD FROM 10 YEARS (2003–2012) OF OBSERVATIONS AT 92 RADIOSONDE STATIONS (UNIT: MILLIMETERS)

| Model | Mean | STD | RMS | Model | Mean | STD | RMS |
|---|---|---|---|---|---|---|---|
| AN_ZW | 5.8 | 35.3 | 35.8 | CH_ZW | -9.6 | 40.3 | 41.5 |
| BA_ZW | -21.2 | 40.5 | 45.7 | EC_ZW | -11.1 | 18.3 | 21.4 |
| BAS_ZW | -1.9 | 33.2 | 33.2 | EG_ZW | -21.2 | 65.1 | 68.4 |
| B70_ZW | -19.4 | 39.6 | 44.1 | GG_ZW | -6.9 | 34.0 | 34.7 |
| B74_ZW | -14.3 | 36.3 | 39.0 | GP_ZW | -12.4 | 43.5 | 45.2 |
| BDN_ZW | -17.3 | 42.9 | 46.2 | HO_ZW | -6.9 | 34.0 | 34.7 |
| BTM_ZW | -16.6 | 36.7 | 40.3 | IF_ZW | 1.6 | 40.2 | 40.2 |
| BL_ZW | -60.4 | 92.4 | 110.4 | SA_ZW | 8.9 | 37.1 | 38.2 |
| CA_ZW | -15.1 | 36.0 | 39.0 | UN_ZW | -10.1 | 62.0 | 62.8 |

## B. Assessment of ZWD Models With Radiosonde

*1) Overall Performance of the ZWD Models:* Table VIII summarizes the detailed statistics of ZWD differences between radiosonde measurements and various ZWD models. In Fig. 3,

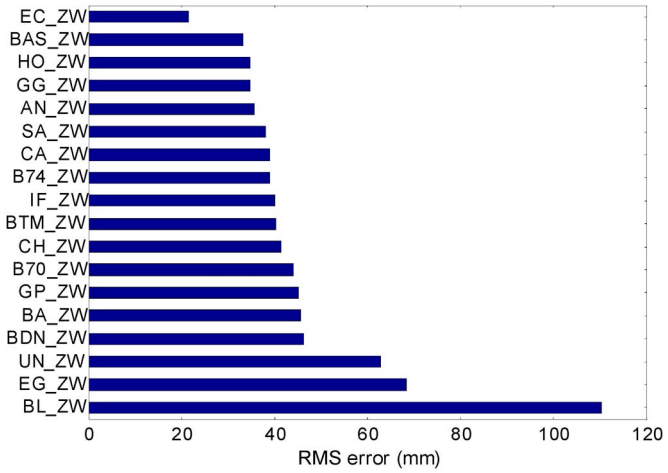


Fig. 3. Ranking of the ZWD models by the size of the rms errors.

the performances of all of the 18 ZWD models are ranked in terms of their rms errors.

It can be seen that the best and worst ZWD models are EC_ZW and BL_ZW, respectively. As highlighted in shadow in Table VIII, their rms errors are 21.4 and 110.4 mm, respectively. The reason for the rather poor performance of BL_ZW can be explained by the fact that only several crude piecewise constant values are used to model the ZWD in BL_ZW (see Section III-D). In general, we can see that all of the models are incompetent to model the ZWD with a high accuracy. Although the size of ZWD usually is only $\sim$10% of ZHD, the rms error of the best ZWD model (EC_ZW, 21.4 mm) is 7.6 times larger than that of the best ZHD model (EC_ZH, 2.8 mm). This clearly illustrates the difficulty of modeling the highly variable ZWD with high accuracy. As shown in Fig. 3, we can also observe that the seven models BAS_ZW, HO_ZW, GG_ZW, AN_ZW, SA_ZW, CA_ZW, and B74_ZW (categorized as group 1) show very similar levels of accuracy. The seven models IF_ZW, BTM_ZW, CH_ZW, B70_ZW, GP_ZW, BA_ZW, and BDN_ZW (categorized as group 2) present similar performances with rms errors varying from 40.2 to 46.2 mm. The rest three models EG_ZW, UN_ZW, and BL_ZW (categorized as group 3) show considerably worse accuracies than the other two groups. The performance of UN_ZW is better than EG_ZW, which demonstrates the improvement in the water vapor pressure prediction in the UN_ZW model. It is worth mentioning that the GP_ZW model in group 2, which requires no actual meteorological observation data, has mean, STD, and rms error of $-12.4$, 43.5, and 45.2 mm, respectively. It performs better than the BA_ZW and BDN_ZW models, both of which need actual meteorological observation data in calculation.

Although EC_ZW achieves the best accuracy in wet delay modeling, it is not suitable for real-time applications because its data could not be obtained in real time. In addition, the use of the BAS_ZW (the second highest accuracy), HO_ZW (or GG_ZW, the third highest accuracy), or AN_ZW (the fourth highest accuracy) models for ZWD modeling is not strongly recommended in practical applications. This is because several parameters in these models (i.e., $\upsilon$ and $\gamma$ in BAS_ZW, $H_w$ in HO_ZW and GG_ZW, and $\alpha$ and $\omega$ in AN_ZW) need to be estimated using local meteorological observations to achieve a better modeling performance. The lack of suitable information on these parameters is a major hindrance in using these models in practice. Instead, the SA_ZW (the sixth highest accuracy), CA_ZW (the seventh highest accuracy), or B74_ZW (the eighth highest accuracy) models are good choices since they require only data of ground surface temperature and water vapor pressure in their modeling.

*2) Seasonal Performance of the ZWD Models:* China region covers a large landmass, and each radiosonde station experiences considerable seasonal variations. Thus, the radiosonde data can be used to evaluate the seasonal performance of the 18 ZWD models. It can be clearly seen in Table IX that the rms errors of the empirical models in winter are significantly smaller than the other seasons. All of the models show that the rms errors in summer are the largest in four seasons. This can be explained that summer and winter are usually the most and least humid seasons of the year, respectively. In addition, it is noted that in the China region the performances of the ZWD models in spring are very similar to those in autumn, with a slightly better accuracy in spring. We can also notice that EC_ZW achieves the best accuracy in all of the four seasons, as highlighted in shadow. In spring, summer, and autumn, the poorest accuracies are yielded by BL_ZW. However, EG_ZW performs the worst in winter among all of the 18 models.

*3) Assessment of the ZWD Models at Different Latitudinal Regions:* The performance evaluation results of the 18 ZWD models in four different latitude zones are presented in Table X. Except the BL_ZW, the rms errors of the ZWD models decrease with latitude increasing. This is consistent with the water distribution fact that northern China (higher latitude regions) is much drier than southern China (lower latitude regions) [56]. The drier atmosphere contains less variable water vapor; thus, it is not a surprise that all of the ZWD models (except BL_ZW) consistently have better modeling accuracies in drier atmosphere. For each latitude region, the ZWD models with the highest and lowest accuracies are highlighted in shadow.

Among the 18 ZWD models, EC_ZW achieves the best performance again in all of the latitude regions. The second best model belongs to BAS_ZW in the latitude regions from 15° N to 45° N. Instead, the SA_ZW model performs the second best in the latitudinal region of 45–55° N with an rms error of 17.5 mm. In addition, the AN_ZW, GG_ZW, GP_ZW, HO_ZW, and IF_ZW models also show comparable performances with the BAS_ZW and SA_ZW models. The two empirical models EG_ZW and UN_ZW show unsatisfactory performances in all of the four regions, with rms errors all larger than 40 mm.

By taking account of both the accuracy and simplicity (using fewer meteorological parameters) of the models for the whole China region (15–55° N), SA_ZW is the first choice to model the ZWD in China. BAS_ZW has a better accuracy than SA_ZW for most part of China (15–45° N); however, it requires much more meteorological parameters than the SA_ZW model. In addition, if surface meteorological observations are difficult to be obtained, we recommend that AN_ZW be exploited to calculate the ZWD corrections with the use of meteorological parameters predicted from the GPT2 model.

TABLE IX
SEASONAL STATISTICS OF DIFFERENCES BETWEEN ZWD DERIVED FROM EMPIRICAL MODELS AND ZWD FROM 10 YEARS (2003–2012) OF OBSERVATIONS AT 92 RADIOSONDE STATIONS (UNIT: MILLIMETERS)

| Model | | Spring | Summer | Autumn | Winter | Model | | Spring | Summer | Autumn | Winter |
|---|---|---|---|---|---|---|---|---|---|---|---|
| | Mean | 4.7 | 12.7 | 4.2 | 2.9 | | Mean | -5.2 | -27.6 | -12.9 | 4.2 |
| AN_ZW | STD | 34.7 | 44.5 | 37.9 | 22.0 | CH_ZW | STD | 38.2 | 51.2 | 41.1 | 24.6 |
| | RMS | 35.0 | 46.3 | 38.1 | 22.2 | | RMS | 38.5 | 58.1 | 43.0 | 25.0 |
| | Mean | -18.9 | -37.2 | -25.5 | -5.5 | | Mean | -12.3 | -14.2 | -10.9 | -7.3 |
| BA_ZW | STD | 38.7 | 49.9 | 41.4 | 26.2 | EC_ZW | STD | 17.9 | 22.8 | 18.5 | 12.1 |
| | RMS | 43.0 | 62.3 | 48.6 | 26.8 | | RMS | 21.7 | 26.9 | 21.4 | 14.1 |
| | Mean | -2.9 | 7.8 | -4.6 | -5.8 | | Mean | -31.7 | 29.6 | -29.5 | -50.2 |
| BAS_ZW | STD | 32.0 | 41.4 | 35.2 | 21.4 | EG_ZW | STD | 57.2 | 69.1 | 64.9 | 35.0 |
| | RMS | 32.1 | 42.1 | 35.5 | 22.2 | | RMS | 65.4 | 75.1 | 71.3 | 61.2 |
| | Mean | -17.1 | -34.4 | -23.4 | -5.6 | | Mean | -7.8 | -2.0 | -11.2 | -5.7 |
| B70_ZW | STD | 38.2 | 49.6 | 40.6 | 25.1 | GG_ZW | STD | 33.0 | 42.7 | 35.8 | 22.8 |
| | RMS | 41.8 | 60.3 | 46.9 | 25.7 | | RMS | 33.9 | 42.8 | 37.5 | 23.5 |
| | Mean | -13.2 | -19.6 | -18.3 | -6.3 | | Mean | -13.6 | -13.6 | -12.1 | -11.0 |
| B74_ZW | STD | 35.8 | 44.8 | 38.0 | 24.4 | GP_ZW | STD | 43.6 | 51.8 | 47.6 | 28.3 |
| | RMS | 38.1 | 48.9 | 42.3 | 25.2 | | RMS | 45.6 | 53.6 | 49.2 | 30.4 |
| | Mean | -15.7 | -23.6 | -22.3 | -8.0 | | Mean | -7.8 | -2.0 | -11.2 | -5.7 |
| BDN_ZW | STD | 40.8 | 54.9 | 44.8 | 27.6 | HO_ZW | STD | 33.0 | 42.7 | 35.8 | 22.8 |
| | RMS | 43.8 | 59.8 | 50.0 | 28.7 | | RMS | 33.9 | 42.8 | 37.5 | 23.5 |
| | Mean | -15.2 | -23.6 | -21.0 | -7.4 | | Mean | -1.2 | 14.5 | -0.8 | -4.3 |
| BTM_ZW | STD | 36.1 | 45.0 | 38.3 | 24.8 | IF_ZW | STD | 39.1 | 50.1 | 41.3 | 26.4 |
| | RMS | 39.2 | 50.8 | 43.7 | 25.8 | | RMS | 39.1 | 52.1 | 41.4 | 26.7 |
| | Mean | -91.7 | -69.1 | -68.3 | -13.2 | | Mean | 7.0 | 19.8 | 6.2 | 4.4 |
| BL_ZW | STD | 87.5 | 107.4 | 93.9 | 47.3 | SA_ZW | STD | 36.2 | 47.0 | 38.8 | 22.8 |
| | RMS | 126.8 | 127.7 | 116.2 | 49.1 | | RMS | 36.9 | 51.0 | 39.3 | 23.3 |
| | Mean | -14.5 | -16.5 | -19.8 | -9.4 | | Mean | -17.0 | 35.9 | -15.4 | -41.5 |
| CA_ZW | STD | 35.5 | 44.5 | 37.9 | 24.5 | UN_ZW | STD | 54.5 | 67.2 | 61.1 | 33.4 |
| | RMS | 38.4 | 47.5 | 42.7 | 26.3 | | RMS | 57.0 | 76.2 | 63.0 | 53.3 |

TABLE X
STATISTICS OF DIFFERENCES BETWEEN ZWD DERIVED FROM EMPIRICAL MODELS AND ZWD FROM 10 YEARS (2003–2012) OF OBSERVATIONS AT 92 RADIOSONDE STATIONS FOR DIFFERENT LATITUDINAL REGIONS (UNIT: MILLIMETERS)

| Model | | Latitudinal Regions (°N) | | | | Model | | Latitudinal Regions (°N) | | | |
|---|---|---|---|---|---|---|---|---|---|---|---|
| | | 15~25 | 25~35 | 35~45 | 45~55 | | | 15~25 | 25~35 | 35~45 | 45~55 |
| | Mean | 15.6 | 12.0 | -1.3 | -6.9 | | Mean | -36.8 | 11.7 | -1.0 | -1.1 |
| AN_ZW | STD | 45.8 | 42.5 | 20.9 | 18.3 | CH_ZW | STD | 61.3 | 46.3 | 23.6 | 21.8 |
| | RMS | 48.4 | 44.2 | 21.0 | 19.6 | | RMS | 71.5 | 47.7 | 23.6 | 21.8 |
| | Mean | -42.5 | -26.8 | -10.4 | -9.7 | | Mean | -11.2 | -12.9 | -9.2 | -9.4 |
| BA_ZW | STD | 54.6 | 46.9 | 25.6 | 24.8 | EC_ZW | STD | 25.1 | 19.8 | 14.3 | 12.6 |
| | RMS | 69.2 | 54.0 | 27.6 | 26.7 | | RMS | 27.5 | 23.6 | 17.0 | 15.7 |
| | Mean | -7.2 | -0.7 | -1.8 | -1.5 | | Mean | 6.5 | -10.2 | -39.9 | -42.3 |
| BAS_ZW | STD | 47.1 | 40.7 | 19.8 | 17.7 | EG_ZW | STD | 75.6 | 75.0 | 41.1 | 36.7 |
| | RMS | 47.6 | 40.7 | 19.9 | 17.8 | | RMS | 75.9 | 75.6 | 57.3 | 56.0 |
| | Mean | -39.2 | -24.2 | -10.1 | -9.3 | | Mean | -15.8 | -6.2 | -5.6 | -5.1 |
| B70_ZW | STD | 54.6 | 46.5 | 24.3 | 22.8 | GG_ZW | STD | 48.2 | 41.0 | 21.1 | 18.5 |
| | RMS | 67.2 | 52.4 | 26.3 | 24.6 | | RMS | 50.7 | 41.5 | 21.8 | 19.2 |
| | Mean | -24.4 | -14.0 | -11.9 | -10.9 | | Mean | -14.4 | -15.5 | -9.6 | -7.9 |
| B74_ZW | STD | 51.3 | 42.9 | 23.3 | 21.9 | GP_ZW | STD | 51.6 | 52.8 | 30.0 | 28.6 |
| | RMS | 56.8 | 45.1 | 26.1 | 24.5 | | RMS | 53.6 | 55.0 | 31.5 | 29.7 |
| | Mean | -29.4 | -17.8 | -12.8 | -12.7 | | Mean | -15.8 | -6.2 | -5.6 | -5.1 |
| BDN_ZW | STD | 63.6 | 50.3 | 26.3 | 25.5 | HO_ZW | STD | 48.2 | 41.0 | 21.1 | 18.5 |
| | RMS | 70.0 | 53.4 | 29.7 | 28.5 | | RMS | 50.7 | 41.5 | 21.8 | 19.2 |
| | Mean | -28.7 | -16.9 | -13.2 | -12.3 | | Mean | 20.4 | 9.2 | -11.6 | -3.8 |
| BTM_ZW | STD | 51.7 | 43.1 | 23.8 | 22.8 | IF_ZW | STD | 50.9 | 48.7 | 21.2 | 17.6 |
| | RMS | 59.2 | 46.3 | 27.2 | 25.9 | | RMS | 54.9 | 49.6 | 24.1 | 18.0 |
| | Mean | 17.7 | -28.0 | -116.1 | -116.9 | | Mean | 19.2 | 15.2 | 0.7 | 2.4 |
| BL_ZW | STD | 78.3 | 87.6 | 65.8 | 58.7 | SA_ZW | STD | 50.0 | 45.2 | 20.3 | 17.3 |
| | RMS | 80.3 | 91.9 | 133.5 | 130.8 | | RMS | 53.6 | 47.7 | 20.3 | 17.5 |
| | Mean | -22.1 | -14.6 | -13.5 | -12.9 | | Mean | 14.7 | -0.5 | -27.1 | -27.1 |
| CA_ZW | STD | 50.3 | 42.7 | 23.2 | 21.8 | UN_ZW | STD | 73.8 | 72.4 | 37.4 | 33.0 |
| | RMS | 54.9 | 45.2 | 26.9 | 25.4 | | RMS | 75.3 | 72.4 | 46.2 | 42.7 |

### C. Validation by GPS PPP

In the assessments presented previously, tropospheric delays derived from the radiosonde were used as benchmarks to evaluate the accuracies of the ZHD and ZWD models. However, from the discussion in Section IV-B, we can notice that radiosonde data are not error free. Thus, the model assessment performed previously is actually dependent on the accuracy of radiosonde measurements. In order to perform an absolute accuracy

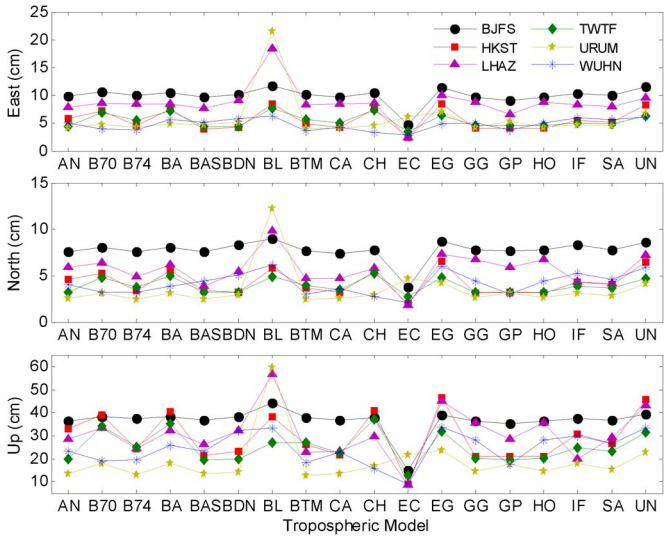


Fig. 4. RMS of PPP kinematic positioning errors.

assessment for all of the tropospheric models, we further evaluate the performances of the models using GPS PPP technique. The PPP is a good method for tropospheric model evaluation since the results obtained for each station are independent [57].

The Positioning And Navigation Data Analyst (PANDA) software package developed by Wuhan University, Wuhan, China, is used to conduct the PPP experiment in this study [58]. In GPS PPP, all of the errors including the tropospheric delay are required to be precisely determined to achieve high-accuracy positioning. In GPS PPP mode, the tropospheric delay can be corrected by two strategies: 1) the tropospheric delay is estimated based on the *a priori* model in the data processing, and 2) the tropospheric delay is directly corrected using an external model [57]. For the first strategy, a common practice is to use an empirical model to directly compute the ZHD. At the same time, the ZWD is parameterized and estimated in the data processing. The PANDA software itself, by default, adopts the first strategy to estimate tropospheric delay. However, in our tests, we did not use the default strategy; instead, we adopted the second strategy. Tropospheric wet delays are no longer estimated with the position coordinates but directly corrected by the tropospheric models. Specifically, the BA_ZH model is used to correct the hydrostatic delay, and the 18 ZWD models are applied to correct the wet delays. This is because of the following: 1) the ZHD is a relatively stable quantity and can be modeled with a high accuracy, and 2) as shown in Fig. 4, the BA_ZH model is the second best ZHD model after EC_ZH. However, the EC_ZH model is not suitable for real-time GPS positioning due to the unavailability of real-time input data. GPS data from six stations (Table XI) for a one-month period, i.e., July 2013, are processed in kinematic mode, with the tropospheric delays calculated by the models. For the five IGS stations (BJFS, LHAZ, TWTF, URUM, and WUHN), the kinematic solutions are assessed by the IGS-provided precise coordinates. In addition, static PPP solutions from the PANDA are used as a reference to evaluate the accuracy of the kinematic solutions for the HKST station.

TABLE XI
LOCATION OF THE SIX GPS STATIONS

| Station name | Latitude (°N) | Longitude (°E) | Height (m) |
|---|---|---|---|
| BJFS | 39.6086 | 115.8925 | 87.4130 |
| HKST | 22.3952 | 114.1842 | 258.6894 |
| LHAZ | 29.6573 | 91.1040 | 3622.0000 |
| TWTF | 24.9536 | 121.1645 | 203.1220 |
| URUM | 43.5900 | 87.6300 | 856.1000 |
| WUHN | 30.5317 | 114.3573 | 28.2000 |

Fig. 4 illustrates the rms of the kinematic PPP positioning errors for the six stations. The abscissa shows the abbreviation code of the 18 ZWD models. The three subgraphs show the rms values for the east, north, and up components, respectively. With the use of tropospheric model, the kinematic PPP accuracy is approximately 5–10 cm in the horizontal and 10–50 cm in the up direction for the tested six stations. As shown in Fig. 4, generally, kinematic PPP solutions using the EC_ZW (ECMWF) and BL_ZW (Black) models have the best and worst performances, respectively. This is in consistency with the assessment presented in the last section. In addition, it is not a surprise that the performance of the EG_ZW (EGNOS) or UN_ZW (UNB3) model is not as good as the other models since these two models use predicted meteorological parameters. Among the six stations, the URUM station gets the highest positioning accuracies. This can be explained that the URUM station is located at Urumqi, a region with semiarid climate. Thus, water-vapor-induced wet delay is not as much as that at the other stations.

In the last section, we classified the 18 ZWD models into three groups according to their accuracy. It is interesting to find that the performances of the 18 models basically match with that classification. The PPP kinematic positioning solutions using the ZWD models of group 1 generally have better accuracies than those using the ZWD models of group 2. This is true for the results obtained from using the ZWD models of group 2 and group 3. Nevertheless, there are some exceptional cases. For instance, the GP_ZW model does not show a good ranking in the assessment presented in Section IV-B (see Fig. 3). However, its performance in kinematic PPP is comparable with BAS_ZW that is ranked as the second best ZWD model in Section IV-B (see Fig. 3). Moreover, for different stations, the performances of some models vary greatly. These discrepancies are explicable by this reason. In the GPS positioning, the zenith delays need to be projected to the line-of-sight direction of the GPS satellite signals with a mapping function (global mapping function [44] is adopted in PANDA software). The mapping function cannot account for the nonisotropic distribution of the atmospheric delay because the water vapor distribution at different azimuths overhead each station is different.

## VI. CONCLUSION

In space geodetic techniques, particularly in today's GNSS applications, it is always scientifically significant and practically important to accurately correct the tropospheric delay to achieve the best possible solutions. The optimal way to correct tropospheric delays is to make observations of atmospheric profiles. However, it is impossible to deploy a large number of

instruments such as radiosonde to obtain atmospheric profiles. In some applications, tropospheric delays with an accuracy of several centimeters are allowed. Based on this realistic consideration, many tropospheric delay models using surface meteorological measurements (including pressure, temperature, and relative humidity) have been developed. In this paper, a comprehensive assessment and analysis of the performance of 9 ZHD models and 18 ZWD models has been performed using the benchmark values derived from 10 years (2003–2012) of observations at 92 radiosonde stations in China.

Our studies show that the ZHD model with the best overall accuracy is EC_ZH with an rms error of 2.8 mm. The BA_ZH, GG_ZH, HO_ZH, BL_ZH, and SA_ZH models also achieve good performances with rms errors ranging from 6.0 to 8.4 mm. For seasonal temporal performance, EC_ZH, BA_ZH, GG_ZH, HO_ZH, BL_ZH, and SA_ZH consistently show good modeling accuracies in all of the four seasons. We have also examined the spatial performances of the models in different latitudinal zones in China. We have found that most of the models perform better in high-latitude regions than in low-latitude regions. Although the EC_ZH achieves the highest accuracy, it is only the best choice for postmission applications. This is because the ECMWF reanalysis data cannot be available in real time and the ECMWF forecasts are very difficult to access. For real-time applications, considering the performance and complexity of all of the models, we recommend that SA_ZD be used to model the ZHD in the China region since it is the simplest one that needs only the surface pressure data. However, if both surface pressure and temperature data are available, the BA_ZH model is recommended. When neither pressure nor temperature data are available or only centimeter-level accuracy is required, GP_ZH is a good choice as we have shown that GP_ZH can achieve an overall accuracy of 11.6 mm in China.

The highly variable nature of the water vapor content in the atmosphere results in the difficulty of modeling the wet delay as well as the hydrostatic delay. The model with the best overall performance is EC_ZW, with an rms error of 21.4 mm. BAS_ZW, HO_ZW, GG_ZW, AN_ZW, and SA_ZW also show relatively good performances with rms errors less than 40 mm. From the perspective of seasonal performance, all of the ZWD models perform better in winter than in summer in the China region. The models in spring show similar performances to those in autumn. In addition, a basically higher accuracy of ZWD modeling can be obtained in high latitudes than in low latitudes. EC_ZW, BAS_ZW, SA_ZW, AN_ZW, GG_ZW, GP_ZW, HO_ZW, and IF_ZW exhibit relatively good accuracies in all of the four latitude zones in China.

In addition to the assessment by radiosonde, we have also tested the 18 ZWD models in the kinematic PPP mode with the ZHD calculated by the BA_ZH model. The performances of the 18 models are generally in good agreement with the accuracy assessment results that use the radiosonde as benchmarks. Generally, the ZWD models in group 1 have better performances than those in group 2 and similarly for the ZWD models in group 2 and group 3. Based on our results, we can conclude the following: 1) for postmission applications, EC_ZW can provide the highest accuracy of ZWD. 2) For real-time applications, a possibility is to use EC_ZW forecasts; however, for most of the users, this kind of data is very difficult to access. Therefore, we recommend SA_ZW as the optimal ZWD model for the China region due to its simplicity and good performance. 3) If there are radiosonde data available, it is recommended to use the radiosonde data to establish a semiempirical Baby model for this region. 4) If no surface meteorological observation is available, the best choice is to employ AN_ZW to compute the ZWD with meteorological parameters provided by the GPT2 model. However, when a more accurate estimate of tropospheric wet delay is required, other techniques such as radiosonde, water vapor radiometer, and GNSS may be considered.

## ACKNOWLEDGMENT

The authors would like to thank the Department of Atmospheric Science, University of Wyoming, Laramie, WY, USA, for providing the observations of 92 radiosonde stations in China, the IGS for providing the GPS data and precise products used in the GPS PPP analysis, Dr. M. Li and W. Li at the GNSS Research Center, Wuhan University, Wuhan, China, for their help in processing the GPS data using the PANDA software, the ECMWF organization scientists for the production of the data used in this research effort, and the three anonymous reviewers and the Editor Prof. A. Plaza for the very constructive comments that greatly improve the quality of this paper.

## REFERENCES

[1] I. M. Ifadis, "Space to Earth techniques: Some considerations on the zenith wet path delay parameters," *Surv. Rev.*, vol. 32, no. 249, pp. 130–144, 1993.

[2] A. Cazenave, P. Gegout, L. Soudarin, and K. Dominh, *Geodetic Results from LAGEOS 1 and DORIS Satellite Data*, vol. 23. Washington, DC, USA: American Geophys. Union, 1993.

[3] G. C. Bower, D. C. Backer, R. L. Plambeck, and M. C. H. Wright, "Removal of tropospheric path length variations in very long baseline interferometry with measurement of tropospheric emission," *J. Geophys. Res.*, vol. 102, no. D14, pp. 16 773-16 781, Jul. 1997.

[4] Z. Li, "Modeling atmospheric effects on repeat-pass InSAR measurements," Ph.D. dissertation, Dept. Land Surveying Geo-Informat., The HongKong Polytechnic Univ., Kowloon, Hong Kong, 2005.

[5] A. Schubert, M. Jehle, D. Small, and E. Meier, "Influence of atmospheric path delay on the absolute geolocation accuracy of TerraSAR-X high-resolution products," *IEEE Trans. Geosci. Remote Sens.*, vol. 48, no. 2, pp. 751–758, Feb. 2010.

[6] T. R. Lauknes, "InSAR tropospheric stratification delays: Correction using a small baseline approach," *IEEE Geosci. Remote Sens. Lett.*, vol. 8, no. 6, pp. 1070–1074, Nov. 2011.

[7] C. Desportes, E. Obligis, and L. Eymard, "One-dimensional variational retrieval of the wet tropospheric correction for altimetry in coastal regions," *IEEE Trans. Geosci. Remote Sens.*, vol. 48, no. 3, pp. 1001–1008, Mar. 2010.

[8] E. E. Altshuler, "Tropospheric range-error corrections for the global positioning system," *IEEE Trans. Antennas Propag.*, vol. 46, no. 5, pp. 643–649, May 1998.

[9] V. de B. Mendes, "Modeling the neutral-atmosphere propagation delay in radiometric space techniques," Ph.D. dissertation, Dept. Geodesy Geomatics Eng., Univ. New Brunswick, Fredericton, NB, Canada, 1998.

[10] M. S. Sudhir, "Investigations into the estimation of tropospheric delay and wet refractivity using GPS measurements," M.S. thesis, Dept. Geomatics Eng., Univ. Calgary, Calgary, AB, Canada, 2003.

[11] Z. Li *et al.*, "Comparative study of empirical tropospheric models for the Hong Kong region," *Surv. Rev.*, vol. 40, pp. 328–341, 2008.

[12] P. Wielgosz, S. Cellmer, Z. Rzepecka, J. Paziewski, and D. A. Grejner-Brzezinska, "Troposphere modeling for precise GPS rapid static positioning in mountainous areas," *Meas. Sci. Technol.*, vol. 22, no. 4, Apr. 2011, Art. ID. 045101.

[13] Z. Liu, M. S. Wong, J. Nichol, and P. W. Chan, "A multi-sensor study of water vapour from radiosonde, MODIS and AERONET: A case study of Hong Kong," *Int. J. Climatol.*, vol. 33, no. 1, pp. 109–120, Jan. 2013.
[14] S. Jin and O. F. Luo, "Variability and climatology of PWV from global 13-year GPS observations," *IEEE Trans. Geosci. Remote Sens.*, vol. 47, no. 7, pp. 1918–1924, Jul. 2009.
[15] M. Fernandes, A. Nunes, and C. Lázaro, "Analysis and inter-calibration of wet path delay datasets to compute the wet tropospheric correction for CryoSat-2 over ocean," *Remote Sens.*, vol. 5, no. 10, pp. 4977–5005, Oct. 2013.
[16] M. Fernandes, C. Lázaro, A. Nunes, and R. Scharroo, "Atmospheric corrections for altimetry studies over inland water," *Remote Sens.*, vol. 6, no. 6, pp. 4952–4997, May 2014.
[17] Z. W. Li *et al.*, "Correcting atmospheric effects on InSAR with MERIS water vapour data and elevation-dependent interpolation model: Correcting atmospheric effects on InSAR," *Geophys. J. Int.*, vol. 189, no. 2, pp. 898–910, May 2012.
[18] C. Delacourt, P. Briole, and J. Achache, "Tropospheric corrections of SAR interferograms with strong topography. Application to Etna," *Geophys. Res. Lett.*, vol. 25, no. 15, pp. 2849–2852, 1998.
[19] H. W. Janes, R. B. Langley, and S. P. Newby, "Analysis of tropospheric delay prediction models: Comparisons with ray-tracing and implications for GPS relative positioning," *Bull. Géod.*, vol. 65, no. 3, pp. 151–161, 1991.
[20] W. Qu, W. Zhu, S. Song, and J. Ping, "Evaluation of the precision of three tropospheric delay correction models," *Chin. Astron. Astrophys.*, vol. 32, no. 4, pp. 429–438, Oct. 2008.
[21] J. D. Dodo and T. O. Idowu, "Regional assessment of the GPS tropospheric delay models on the African GNSS network," *J. Emerg. Trends Eng. Appl. Sci.*, vol. 1, no. 1, pp. 113–121, Oct. 2010.
[22] A. Tuka and A. El-Mowafy, "Performance evaluation of different troposphere delay models and mapping functions," *Measurement*, vol. 46, no. 2, pp. 928–937, Feb. 2013.
[23] W. Luo, Z. Liu, and M. Li, "A preliminary evaluation of the performance of multiple ionospheric models in low- and mid-latitude regions of China in 2010–2011," *GPS Solut.*, vol. 18, no. 2, pp. 297–308, Apr. 2014.
[24] S. Song *et al.*, "Near real-time sensing of PWV from SGCAN and the application test in numerical weather forecast," *Chin. J. Geophys.*, vol. 47, no. 4, pp. 719–727, 2004.
[25] Y. Bi, J. Mao, and C. Li, "Preliminary results of 4D water vapor tomography in the troposphere using GPS," *Adv. Space Res.*, vol. 23, no. 4, pp. 551–560, 2006.
[26] Z. Liu and M. Li, "The first PPP-based GPS water vapor real-time monitoring system in Pearl-River-Delta region, China," in *China Satellite Navigation Conference (CSNC) 2013 Proceedings*, vol. 243, J. Sun, W. Jiao, H. Wu, and C. Shi, Eds. Berlin, Germany: Springer-Verlag, 2013, pp. 71–87.
[27] J. Askne and H. Nordius, "Estimation of tropospheric delay for microwaves from surface weather data," *Radio Sci.*, vol. 22, no. 3, pp. 379–386, May/Jun. 1987.
[28] E. K. Smith and S. Weintraub, "The constants in the equation for atmospheric refracrive index at radio frequencies," *J. Res. Nat. Bur. Standards*, vol. 50, no. 1, pp. 39–41, Jan. 1953.
[29] A. L. Buck, "New equations for computing vapor pressure and enhancement factor," *J. Appl. Meteorol.*, vol. 20, no. 12, pp. 1527–1532, Dec. 1981.
[30] R. J. Ross and W. P. Elliott, "Tropospheric water vapor climatology and trends over North America: 1973–93," *J. Clim.*, vol. 9, no. 12, pp. 3561–3574, Dec. 1996.
[31] J. M. Rüeger, "Refractive index formulae for radio waves," in *Proc. FIG XXII Int. Congr.*, Washington, D.C. USA, 2002, pp. 1–13.
[32] J. Saastamoinen, "Atmospheric correction for the troposphere and stratosphere in radio ranging of satellites," *Geophys. Monogr. Ser.*, vol. 15, pp. 247–251, 1972.
[33] J. L. Davis, T. A. Herring, I. I. Shapiro, A. E. E. Rogers, and G. Elgered, "Geodesy by radio interferometry: Effects of atmospheric modeling errors on estimates of baseline length," *Radio Sci.*, vol. 20, no. 6, pp. 1593–1607, Dec. 1985.
[34] J. Saastamoinen, "Contributions to the theory of atmospheric refraction: Part II. Refraction corrections in satellite geodesy," *Bull. Geod.*, vol. 107, pp. 13–34, 1973.
[35] H. B. Baby, P. Golé, and J. Lavergnat, "A model for the tropospheric excess path length of radio waves from surface meteorological measurements," *Radio Sci.*, vol. 23, no. 6, pp. 1023–1038, Nov./Dec. 1988.
[36] H. Hopfield, "Two-quartic tropospheric refractivity profile for correcting satellite data," *J. Geophys. Res.*, vol. 74, no. 18, pp. 4487–4499, 1969.
[37] H. Hopfield, "Tropospheric effect on electromagnetically measured range: Prediction from surface weather data," *Radio Sci.*, vol. 6, no. 3, pp. 357–367, 1971.
[38] H. D. Black, "An easily implemented algorithm for the tropospheric range correction," *J. Geophys. Res.*, vol. 83, no. B4, pp. 1825–1828, Apr. 1978.
[39] C. C. Goad and L. L. Goodman, "A modified Hopfield tropospheric refraction correction model," presented at the Fall Annual Meeting American Geopgysical Union, San Francisco, CA, USA, 1974.
[40] CLAR, "*U.S. Standard Atmosphere Supplements, 1966*." Superintendent of Documents, U.S. Government Printing Office, 1966.
[41] A. Farah, "Assessment of UNB3M neutral atmosphere model and EGNOS model for near-equatorial-tropospheric delay correction," *J. Geomatics*, vol. 5, no. 2, pp. 67–72, Oct. 2011.
[42] N. Penna, A. Dodson, and W. Chen, "Assessment of EGNOS tropospheric correction model," *J. Navig.*, vol. 54, no. 1, pp. 37–55, 2001.
[43] R. Leandro, M. C. Santos, and R. B. Langley, "*UNB neutral atmosphere models: Development and performance*," in *Proc. ION NTM*, 2006, pp. 18–20.
[44] J. Boehm, A. Niell, P. Tregoning, and H. Schuh, "Global mapping function (GMF): A new empirical mapping function based on numerical weather model data," *Geophys. Res. Lett.*, vol. 33, no. 7, pp. 1–4, Apr. 2006.
[45] K. Lagler, M. Schindelegger, J. Böhm, H. Krásná, and T. Nilsson, "GPT2: Empirical slant delay model for radio space geodetic techniques," *Geophys. Res. Lett.*, vol. 40, no. 6, pp. 1069–1073, Mar. 2013.
[46] D. P. Dee *et al.*, "The ERA-Interim reanalysis: Configuration and performance of the data assimilation system," *Q. J. R. Meteorol. Soc.*, vol. 137, no. 656, pp. 553–597, Apr. 2011.
[47] A. Berman, "The prediction of Zenith range refraction from surface measurements of meteorological parameters," Jet Propulsion Lab., California Inst. Technol., Pasadena, CA, USA, JPL Tech. Rep. 32-1602, 1976.
[48] P. Callahan, "Prediction of tropospheric wet-component range error from surface measurements," Jet Propulsion Lab., California Inst. Technol., Pasadena, CA, USA, JPL Tech. Rep. 32-1526, 1973.
[49] C. C. Chao, "A new method to predict wet zenith range correction from surface measurements," Jet Propulsion Lab., California Inst. Technol., Pasadena, CA, USA, Tech. Rep. 32-1602, 1971.
[50] Guide to Meteorological Instruments and Methods of Observation, World Meteorological Organization, Geneva, Switzerland, 2008.
[51] A. E. Niell *et al.*, "Comparison of measurements of atmospheric wet delay by radiosonde, water vapor radiometer, GPS, and VLBI," *J. Atmosp. Ocean. Technol.*, vol. 18, pp. 830–850, 2001.
[52] F. Li, Y. Xing, and R. Yang, "Analysis on measure ability of Chinese-developed GPS sounding technology," *Meteorol. Sci. Technol.*, vol. 40, no. 4, pp. 513–519, 2012.
[53] Q. Guo, P. Zhao, Y. Zhang, and F. Liu, "Technical improvement and experimental analysis of GTS1 radiosonde," *Meteorol. Sci. Technol.*, vol. 41, no. 2, pp. 254–258, 2013.
[54] W. Li, P. Zhao, Q. Guo, and M. Wang, "The international radiosonde intercomparison results for China-made GPS radiosonde," *J. Appl. Meteorol. Sci.*, vol. 22, no. 4, pp. 453–462, 2011.
[55] J. Nash, T. Oakley, H. Vömel, and W. Li, "WMO intercomparison of high quality radiosonde systems," World Meteorol. Org., Yangjiang, China, 2011.
[56] P. Zhai and R. E. Eskridge, "Atmospheric water vapor over China," *J. Clim.*, vol. 10, no. 10, pp. 2643–2652, 1997.
[57] T. Hadas, J. Kaplon, J. Bosy, J. Sierny, and K. Wilgan, "Near-real-time regional troposphere models for the GNSS precise point positioning technique," *Meas. Sci. Technol.*, vol. 24, no. 5, May 2013, Art. ID. 055003.
[58] J. Liu and M. Ge, "PANDA software and its preliminary result of positioning and orbit determination," *Wuhan Univ. J. Nat. Sci.*, vol. 8, no. 2B, pp. 603–609, 2003.

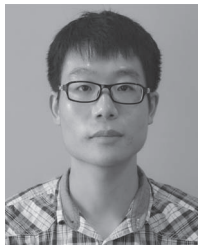

**Biyan Chen** (S'15) received the B.S. degree in surveying engineering from the University of Science and Technology Liaoning, Liaoning, China, in 2009 and the M.S. degree in geodesy and survey engineering from Central South University, Hunan, China, in 2012. He is currently working toward the Ph.D. degree in the Department of Land Surveying and Geo-Informatics, The Hong Kong Polytechnic University, Kowloon, Hong Kong.

His current research interests include GPS/GNSS meteorology, water vapor tomographic technique with multisensor data, and weather forecasting.

**Zhizhao Liu** received the B.Sc. degree in surveying engineering from Jiangxi University of Science and Technology, Ganzhou, China, in 1994, the M.Sc. degree in geodesy from Wuhan University, Wuhan, China, in 1997, and the Ph.D. degree in geomatics engineering from the University of Calgary, Calgary, AB, Canada, in 2004.

He is currently an Associate Professor with the Department of Land Surveying and Geo-Informatics, The Hong Kong Polytechnic University, Kowloon, Hong Kong. He is a guest Professor with Liaoning Technical University, Huludao, China, and Wuhan University. His research interests include new algorithm development for precise Global Positioning System (GPS) and Global Navigation Satellite System (GNSS), GPS/GNSS precise point positioning (PPP), ionosphere modeling and scintillation monitoring, tropospheric remote sensing and modeling, and GPS/GNSS meteorology. He has over 20 years of experience in GPS/GNSS research. His group developed China's first GPS PPP-based Precipitable Water Vapor Real-time Monitoring System in the Pearl-River-Delta region in 2012. His research group established Hong Kong's first GPS/GNSS-radiosonde water vapor sounding collocation system in 2013 in collaboration with Hong Kong Observatory. In 2012, his group developed Hong Kong's first GPS/GNSS-based ionosphere scintillation monitoring system (two stations deployed in South and North Hong Kong) with his collaborators.

Dr. Liu was the recipient of the inaugural Early Career Award of the Hong Kong Research Grants Council (RGC), Hong Kong, in 2012 and was the recipient of the inaugural Best Conference Paper of the China Satellite Navigation Conference (CSNC), China, in 2013. In 2014, he was nominated by the Hong Kong Observatory for the World Meteorological Organization (WMO) "Norbert Gerbier-MUMM International Award for 2015" for his paper that has developed a method to evaluate the absolute accuracy of water vapor measurements.